



# An analytical approach to assess the variation of lubricant supply to the cutting tool during MQL assisted high speed micromilling



Suman Saha, Sankha Deb, Partha Pratim Bandyopadhyay\*

Department of Mechanical Engineering, Indian Institute of Technology Kharagpur, Kharagpur, West Bengal, 721302 India

## ARTICLE INFO

Associate Editor: E. Budak

### Keywords:

Minimum quantity lubrication  
MQL  
Cutting fluid  
Droplet  
Micromilling  
Chip tool contact length

## ABSTRACT

Minimum Quantity Lubrication (MQL) assisted micromilling showed promising results in improving machinability. However, no past work is available on the adequacy of MQL oil flow rate, and its variation with process parameters during micro end milling. A higher oil flow rate can undesirably increase the volumetric disposal rate of cutting oil to the environment without appreciable change in machinability. Accordingly, this article explores whether a given supply of MQL lubricant is abundant, adequate or deficient for the process for various spindle speeds and axial depths. An analytical model is developed by considering the geometry of the actual rounded-edge of the micro end milling tool and elastic regain of the workpiece material, and interrelating these with the characteristics of the MQL jet and oil droplets. For fixed nozzle angles, the interaction between oil droplets and micro end milling tool rotating at varying speeds is further explored. It is observed that 6 mL/hr MQL oil flow rate is abundant for 15,000 rpm spindle speed, adequate for 25,000 rpm, and deficient for higher speeds. The roles of abundant and deficient MQL oil supply on surface quality and burr formation in micromilling of poly (methyl methacrylate) (PMMA) samples are also investigated by comparing with the corresponding results obtained in dry cutting. It is concluded that higher axial depth of cut primarily does not cause lubricant deficiency, but such deficiency is perceived only when speed exceeds a certain limit. Proper lubrication can effectively reduce the bottom-surface roughness of the machined slot. Also, the difference between top-burr width during dry and MQL assisted micromilling in the up milling side decreases with an increase in the oil deficiency. Finally, it is concluded that either the speed should be kept low or the flow rate should be increased to produce an improved lubrication effect at higher axial depths.

## 1. Introduction

Now-a-days the manufacturing industries are swiftly adopting sustainable production strategy with the goal of utilizing minimal resources for meeting the actual demand without harming the environment. Minimum usage of raw material and energy for production of intended goods as well as minimum discharge of inorganic elements to the environment are the main themes of sustainable production (Schneider et al., 2019). Such a production strategy not only comply with the strict government regulations and minimizes pollution risk but also cuts down production cost significantly. Mechanical micro-machining process employs a miniaturized cutting tool with sharp cutting edges in order to remove excess materials from the workpiece in the form of micro-chips to fabricate complex micro-features like straight and curved slots, pockets, webs, pillars, fins, dimples, textures, form-free surfaces, etc. with reasonable dimensional accuracy. As a micro-fabrication process, mechanical micromilling inherently fulfils two

crucial aspects of sustainable production, namely minimizations of raw material usage and energy requirement for production. Accordingly, application of cutting fluid is one crucial area to consider in this regard as cutting fluid sometimes helps improving machining performance but at the cost of pollution risk.

Several fluid delivery techniques during metal cutting were discussed by Krolczyk et al. (2019) and classified the cutting environment as dry, minimum quantity lubrication (MQL), high-pressure liquid jet flood cooling, cryogenic cooling and biodegradable-oil based cooling. In addition, solid lubricant and chilled-air based cutting were investigated by several researchers (Abellan-Nebot and Rogero, 2019). Bruschi et al. (2016) investigated the micromilling performance during machining Ti-6Al-4V samples in three different cooling strategies, namely dry, cryogenic and MQL. Dry cutting outperformed MQL assisted cutting in terms of surface roughness but at the cost of increased nano-hardness of the machined surface. Potential benefits of MQL assisted micromilling were highlighted by several researchers. Rezaei

\* Corresponding author.

E-mail address: [ppb@mech.iitkgp.ac.in](mailto:ppb@mech.iitkgp.ac.in) (P.P. Bandyopadhyay).

<https://doi.org/10.1016/j.jmatprotec.2020.116783>

Received 10 February 2020; Received in revised form 14 May 2020; Accepted 23 May 2020

Available online 28 May 2020

0924-0136/ © 2020 Elsevier B.V. All rights reserved.

Nomenclature			
$r_e$	Edge radius of the cutting tool ( $\mu\text{m}$ )	Q	MQL oil flow rate ( $\mu\text{m}^3/\text{s}$ )
$f_z$	Feed per flute ( $\mu\text{m}/\text{tooth}$ )	$\rho_{\text{droplet}}$	Droplet density or number of oil droplets per unit area per second ( $\mu\text{m}^{-2} \text{s}^{-1}$ )
N	Spindle speed (rpm)	$V_{\text{droplet}}$	Volume of each droplet when droplets are within MQL jet ( $\mu\text{m}^3$ )
$\gamma$	Rake angle of the cutting tool ( $^\circ$ )	$N_{\text{droplet}}$	Total number of droplets produced per second ( $\text{s}^{-1}$ )
$\alpha$	Clearance angle of the cutting tool ( $^\circ$ )	$R_{\text{droplet}}$	Radius of each spherical droplet ( $\mu\text{m}$ )
$\Psi$	Helix angle of the cutting tool ( $^\circ$ )	$V_{\text{droplet-surface}}$	Volume of each droplet when deposited on solid surface ( $\mu\text{m}^3$ )
$\beta$	Shear angle ( $^\circ$ )	a	Height of a droplet when it is deposited on surface ( $\mu\text{m}$ )
$a_1$	Uncut chip thickness at the end of up milling for each tool rotation ( $\mu\text{m}$ )	b	Radius at base of a droplet when it is deposited on surface ( $\mu\text{m}$ )
$a_2$	Chip thickness at the end of up milling for each tool rotation ( $\mu\text{m}$ )	$A_{\text{wet}}$	Wetting area by each droplet ( $\mu\text{m}^2$ )
$h_i$	Instantaneous uncut chip thickness ( $\mu\text{m}$ )	$T_{\text{dis}}$	Disengagement period for each cutting edge (s)
$h_{\text{min}}$	Minimum uncut chip thickness required for smooth shearing ( $\mu\text{m}$ )	Z	Number of flutes present in the cutting tool
$h_{\text{er}}$	Thickness of the elastic recovery part at the finished surface ( $\mu\text{m}$ )	$A_{T1}$	Target area for MQL deposition parallel to the reference plane ( $\mu\text{m}^2$ )
$\epsilon_e$	Elastic strain of the workpiece material (mm/mm of thickness)	$A_{T2}$	Target area for MQL deposition perpendicular to the reference plane ( $\mu\text{m}^2$ )
$L_1, L_2, L_3$	Contact lengths in different segments between chip-tool-workpiece ( $\mu\text{m}$ )	$T_{\text{ex}}$	Exposure time of corresponding target area towards MQL jet (s)
$a_p$	Axial depth of cut ( $\mu\text{m}$ )	$\theta_i$	Instantaneous angular position of the cutting edge in disengaged period ( $^\circ$ )
$a_h$	Actual length of helical cutting edge within the axial depth of cut ( $\mu\text{m}$ )	$N_{\text{useful-droplet}}$	Number of useful oil droplets that strike the concerned target areas
$A_{\text{lub}}$	Intended lubricated area surrounding each cutting edge ( $\mu\text{m}^2$ )	$\Delta N$	Indicates deficiency or abundancy in lubrication in terms of number of droplets
$D_{\text{jet}}$	Diameter of air oil mixture MQL jet ( $\mu\text{m}$ )	$\zeta$	Chip reduction coefficient (ratio between chip thickness to uncut chip thickness)
$A_{\text{jet}}$	Cross-sectional area of air oil mixture MQL jet ( $\mu\text{m}^2$ )	$R_a$	Average surface roughness (nm)
$V_{\text{jet}}$	Velocity of air oil mixture MQL jet ( $\mu\text{m}$ )	$W_B$	Average top-burr width ( $\mu\text{m}$ )
$\omega$	Apex angle of the right cone formed by MQL jet ( $^\circ$ )		
S	Linear distance from nozzle tip to the tool axis ( $\mu\text{m}$ )		

et al. (2017) showed that MQL application has palpable influence on the size effect phenomenon. It was observed that MQL assistance can considerably reduce minimum uncut chip thickness required for the transition from ploughing to shearing for chip formation in micromilling. While this minimum uncut chip thickness remained in between 25–49 % of the edge radius in dry micromilling, the same reduced to 15–34 % in MQL assisted cutting.

During micromilling of Ti-6Al-4 V samples in three different environments (dry, jet flooding and MQL), Vazquez et al. (2015) observed that flood cooling undesirably hampers the dimensional accuracy of the feature without any appreciable impact on cutting performance. Average burr height and surface roughness in jet flood cooling were also found inferior to dry cutting. On the other hand, cutting oil consumption in flood cooling was 47 times higher as compared to the same for MQL. The temperature in micromilling remains considerably low ( $\sim 120^\circ\text{C}$  for 100 m/min velocity while cutting Ti-6Al-4 V), and this hot zone is confined in a localized region (i.e. without any bulk heating). Hence, it was argued that flood cooling is not useful in micro-cutting from economics and sustainability aspects. Li and Chou (2010) observed over 60 % reduction in tool flank wear in MQL based micromilling of SKD 61 steels as compared to dry cutting. Uzun et al. (2013) examined effects of MQL on micro-end milling tool wear and observed that MQL oil helps preventing chip adherence and built-up edge formation on the tool. Mittal et al. (2017) showed that stability in high speed micromilling is also affected by the lubrication, especially when rotational speed is above 50,000 rpm. Proper lubrication can improve chatter based dynamic stability limit by as much as 20 %. Jun et al. (2008) showed that application of atomized cutting fluid in high speed micromilling offers proper assistance in chip evacuation that discourages chip clogging and helps improving surface quality. Liao et al. (2020) carried out micromilling experiments in different cutting

environments and observed that surface roughness in MQL assisted cutting remains more-or-less equal to that of flood cooling but significantly less than that obtained in dry cutting.

A wide variety of MQL oil flow rate is also used in literature. Li and Chou (2010) varied the oil flow rate between 1.88–7.5 mL/h. Rezaei et al. (2017) performed micromilling experiments with UNILUBE 2032 MQL oil at 15 mL/h flow rate. Uzun et al. (2013) used 150 mL/h oil flow rate. Even though several works on micromilling in MQL cutting environment have been carried out by different proponents, there is no such work focusing on the interaction of MQL oil droplet with the micro end mill. No past work is also available on the adequacy of flow rate of MQL oil, and its variation with process parameters. Accordingly, a further refinement in MQL oil delivery strategy is quantification of “adequate” oil flow rate maintaining balance between the machining performance and discharged oil volume. This article attempts to explore whether a given supply of MQL lubricant is adequate for the process under various parameters when cutting fluid is delivered at the trailing end of the tool. Objectives of this investigation are listed below.

- 1 To analytically estimate the chip-tool-workpiece contact area where lubrication is desired for each cutting edge of the micro-end mill considering the rounded edge of the tool and elastic regain of the workpiece material.
- 2 To study the characteristics of MQL jet and the oil droplets for finding out the number of droplets required to properly lubricate the intended contact area.
- 3 To investigate whether the MQL oil supply is adequate for a fixed nozzle angle and flow rate but varying spindle speeds and axial depths. The final goal is to characterize the oil supply as abundant, adequate or deficient for a given set of parameters.
- 4 To investigate the role of abundant and deficient MQL oil supply on

the surface quality and burr formation during micromilling of PMMA samples. Result obtained in dry cutting are used for comparison purpose.

## 2. Material and methods

Poly(methyl methacrylate) (abbreviated as PMMA) has emerged as a preferred substrate for a wide variety of microfluidic and optical devices including micro-chips, micro-valves, micro-pumps, micro-sensors, and micro-lens (Pourmand et al., 2018) for its intrinsic qualities like excellent optical transparency, low price, adequate mechanical strength, chemical stability, less hydrophobicity, and suitability for rapid prototyping (Zhang et al., 2009). As highlighted by Wang and Fu (2018), such applications frequently desire miniaturized features, like micro-channels having width typically below 500  $\mu\text{m}$  and length more than 2 mm, circular pocket type reservoirs having diameter typically 2–5 mm, etc. Usually, depth of such features varies from 0.01 – 0.20 mm. In the present study, PMMA samples of size  $20 \times 20 \times 10 \text{ mm}^3$  are selected for carrying out micromilling experiments. PMMA being a soft material is intentionally selected for the validation purpose as it does not promote rapid tool wear and deflection of the slender micro-end milling tool (run-out), even in dry micromilling. This ensures uniform thickness of all the chips collected for each slot, as discussed later in Section-4. The effects of abundant, adequate and deficient lubrication conditions in MQL assisted cutting on surface roughness and burr formation are judged in this article by comparing the results with the corresponding cases of dry micromilling. The reduced tendency of tool wear and run-out makes such comparison appropriate and free from ancillary influences.

Mounting the samples on the mechanical vice, flatness of the top surface is ensured as any inclination may result in a gradual change in the axial depth during machining. A rectangular island of 5 mm width, 20 mm long and 2 mm height (Fig. 1) is made on each as-received sample by end-milling with a 5 mm diameter cutter. All micromilling experiments are performed on this island using a KERN Evo CNC machining centre (KERN Microtechnik GmbH, Germany). Full immersion (total radial depth of cut is equal to tool diameter) straight slots of 5 mm long are micro-milled using varying cutting speed and axial depth (Table 1). The feed per flute is, however, kept constant at  $4.0 \mu\text{m}/\text{flute}$  in all experiments. This feed value is selected to ensure smooth shearing by every cutting edge in each rotation, as discussed in section-3.2.

All of the experiments are carried out separately in two distinct cutting environments, namely dry cutting and minimum quality lubrication (MQL) assisted cutting. In dry cutting, no cutting fluid is supplied additionally. In MQL based cutting, UNILUBE 2032 cutting oil (UNILUBE, Switzerland) is continuously delivered via an inbuilt ECOLUBE delivery system using two nozzles directed towards the cutting zone (Fig. 1). Dehumidified air, at a pressure of 7.0 bar, is internally mixed with cutting oil prior to delivery. The nozzles are positioned in such a way that cutting fluid can be delivered along the feed direction at an angle of  $45^\circ$  in each side. Both the nozzles are also placed at  $60^\circ$  angle with the Z-axis, matching with the helix angle of the tool. A nozzle-tool distance of 10 mm is maintained throughout the experiments. Such a configuration maintains the uniformity in fluid delivery between up and down milling sides, and at the same time, delivers cutting fluid in the disengaged side of the cutting edge. Several properties of MQL fluid are provided in Table 2. The contact angle, diameter and height of deposited droplet are measured using a contact-angle meter (DMs-401, KYOWA, Japan) in two different planes using an additional scale. An average of 10 measurements are considered for analysis.

TiAlN coated tungsten carbide micro-end mills (AXIS-Microtools, India) of diameter 500  $\mu\text{m}$  are employed for this investigation. Values of basic features of the tool are provided in Table 3. As shown in Fig. 2, helix angle and edge radius of the tool are measured from scanning electron microscope (SEM) (EVO 18, ZEISS) images, following the

technique discussed by Baburaj et al. (2017). One fresh tool is assigned for cutting each slot with pre-defined set of process parameters. Tool overhang length is kept unchanged across all experiments to eliminate chances of dynamic effects. Chips are also collected during micromilling in every pass. Such chips are observed under SEM and analysed further. Similarly, the micro-milled slots are observed under the SEM to measure burr dimensions, and also to spot apparent surface irregularity. Such SEM images are further analysed using AxioVision software. A non-contact type 3-D optical profiler (CCI MP, Taylor Hobson, UK) is used to scan the slot surface for measuring surface roughness following the procedure suggested by Medeossi et al. (2018). Before scanning, the slots are ultrasonically cleaned in water medium to remove loosely deposited chips. An imaginary section along the feed direction is taken at the middle of the slot on the scanned surface, and the centre line average roughness ( $R_a$ ) value is measured on this plane for a sample length of 1.0 mm.

## 3. Interaction between MQL droplets and rotating micro-end milling tool for varying parameters

### 3.1. Basics for the modelling

Irrespective of the delivery technique, the cutting fluid primarily serves two different functions in machining. It acts as a lubricant to reduce dynamic co-efficient of friction between the contact surfaces. Thus lubrication action of the cutting fluid works during chip formation. Cutting fluid also acts as a coolant and thereby takes away generated heat from the machining zone. Vazquez et al. (2015) measured the temperature at a localized point in dry micromilling of Ti-6Al-4 V at 30,000 rpm, which was found to be around  $130^\circ\text{C}$ . This temperature rise is expected to be even less during micromilling of PMMA samples as heat generation is proportional to the strength of the material. Friedrich

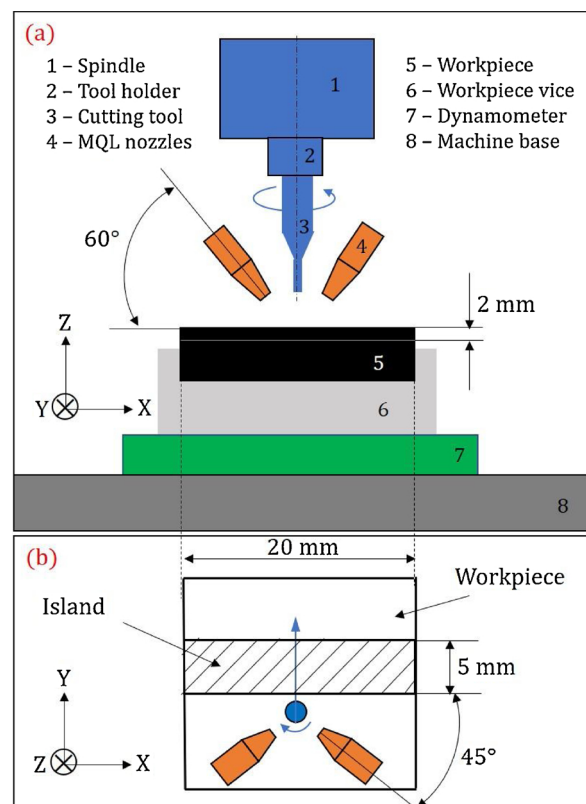


Fig. 1. Schematic representation of machining set-up in (a) X-Z, and (b) X-Y plane.

**Table 1**  
Process parameters used in this work.

Parameter	Nature	Value
Spindle speed	Variable	15,000, 25,000, 35,000, 45,000 rpm
Axial depth of cut	Variable	20, 40, 60, 80 $\mu\text{m}$
Feed per flute	Fixed	4.0 $\mu\text{m}/\text{flute}$
Radial depth of cut	Fixed	500 $\mu\text{m}$
Cutting environment	Variable	Dry, MQL

**Table 2**  
Parameters related to MQL fluid delivery and oil properties.

Feature	Value
Number of delivery nozzles	2
Cutting oil	UNILUBE 2032
Oil kinematic viscosity	~ 35 cSt
Total oil flow rate	6 mL/hr ( $1.67 \times 10^9 \mu\text{m}^3/\text{s}$ )
Air pressure	7.0 bar
Nozzle-Tool Distance (NTD)	10 mm
Nozzle angle in X-Y plane	45° (behind the tool)
Nozzle angle in X-Z plane	60° (w.r.t work surface)

**Table 3**  
Features of the micro-end milling tool used in this study.

Feature	Value
Type	2-flute flat-end micro-end mill
Tool material	TiAlN coated Tungsten Carbide
Tool diameter	0.5 mm
Helix angle	30°
Rake angle	13.5 $\pm$ 0.5°
Clearance angle	19.0 $\pm$ 0.8°
Bottom clearance angle	9.0 $\pm$ 0.2°
Edge radius	1.36 $\pm$ 0.08 $\mu\text{m}$

(2000) also indicated that the temperature rise is hardly 10–20 °C in micromilling of PMMA when cutting velocity is typically below 100 m/min. Such a small temperature has negligible impact on cutting performance, particularly when the cutting length is limited to 5 mm. As cooling effect is not imperative, so it is undesirable to supply MQL oil on the surrounding areas of the cutting zone to continuously cool down the entire area. However, it is necessary to supply oil on the chip-tool-

workpiece contact areas to improve lubrication action. Accordingly, an analytical model is first developed (Fig. 3) based on the following assumptions to understand the MQL oil droplet deposition scenario on the cutting edge for varying parameters.

- The minimum uncut chip thickness ( $h_{\min}$ ) is constant as the tool and workpiece are unchanged, and this  $h_{\min}$  is equal to 33 % of  $r_e$  (i. e.  $h_{\min} = 0.45 \mu\text{m}$ ).
- Rake surface of the tool is flat over the short plastic contact length with chip (i.e. rake angle is constant over the contact length).
- There are two identical nozzles that deliver MQL air-oil mixture to the cutting zone at constant flow rate and mixing ratio. Outlet of such nozzles is considered as a point (i.e. nozzle is a point source).
- MQL oil deposited on a cutting edge during the disengagement period is completely utilized during the next engagement period (i.e. no residue of oil is left).
- Only oil droplets participate in lubrication action. Compressed air that acts as carrier gas has no role on lubrication.
- There is no post-impact rebounding and shattering of the MQL oil droplets for a medium nozzle-tool distance of 10 mm.
- MQL oil droplet density and droplet radius are constants irrespective of the angular location of the cutting edge during the rotation of the tool, since the nozzle-tool distance is significantly higher than the tool diameter.

### 3.2. Chip-tool contact length and lubricating area for rounded cutting edge

In full immersion straight slot milling, the contact between a cutting edge and workpiece happens for half a rotation, while the same cutting edge remains disengaged from the cutting zone for the rest 180°. During this contact period, up milling (conventional milling) and down milling (climb milling) occur in sequence for a quarter-cycle. Chip thickness also gradually changes during the rotation of the cutting edge (Sahoo et al., 2020). The maximum uncut chip thickness is, however, equal to the feed per flute ( $f_z$ ). On the other hand, shearing of the workpiece material initiates only when the instantaneous uncut chip thickness ( $h_i$ ) is above a minimum uncut chip thickness ( $h_{\min}$ ) value. Below this  $h_{\min}$ , rubbing and ploughing predominate that lead to elastic-plastic deformation of the workpiece material. A series of investigations have been carried out by several researchers to estimate this  $h_{\min}$  value. Oliveira et al. (2015) determined that  $h_{\min}$  value lies between 25 – 33% of  $r_e$  irrespective of the workpiece material. It was also recommended to

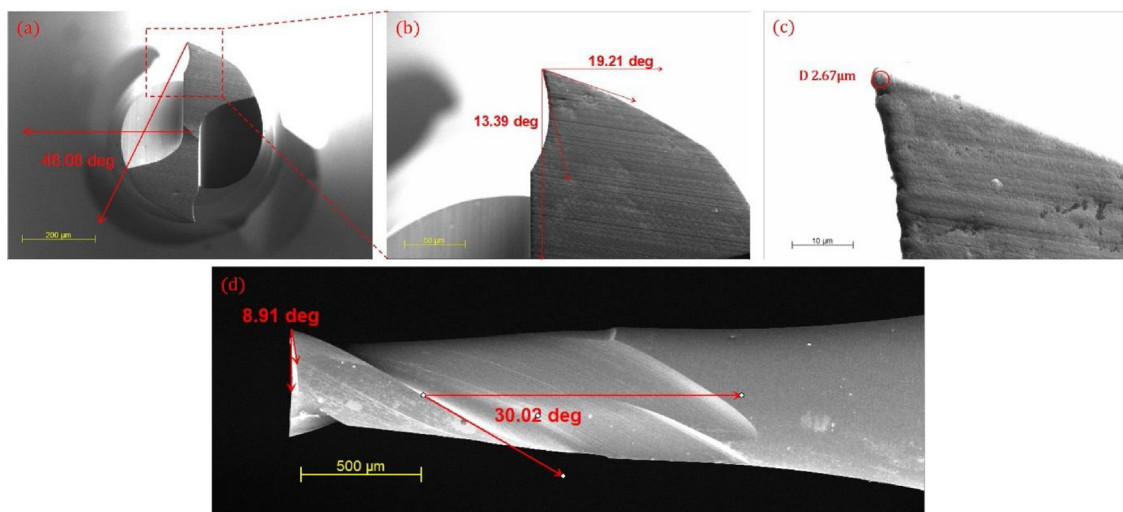


**Fig. 2.** SEM images of the micro-end milling tool (a) top-view, (b) enlarged top-view of a cutting edge showing rake angle of 13.39° and primary clearance angle of 19.21°, (c) enlarged view of tool-tip showing edge radius of 1.33  $\mu\text{m}$ , and (d) side view of the tool showing helix angle of 30° and bottom clearance angle of 8.9°.

## Finding out abundant, adequate, and deficient lubrication conditions

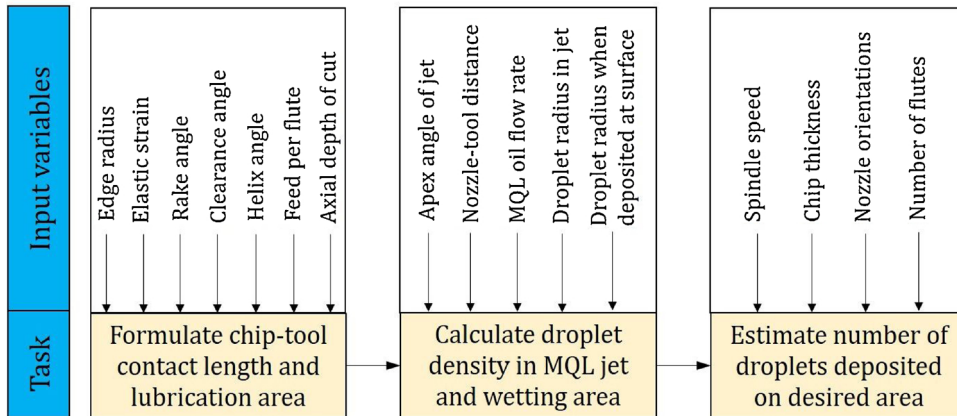


Fig. 3. Steps to develop the model for estimating adequate flow rate of cutting fluid.

select a significantly higher feed value than the one corresponding to the  $h_{min}$  value for achieving better surface integrity. For the selected micro-end milling tool having  $r_e = 1.36 \mu m$ , the intended  $h_{min}$  is  $0.45 \mu m$  (assuming 33 % of  $r_e$ ). Here,  $f_z$  value is set to  $4 \mu m/flute$  in order to ensure chip formation by each cutting edge in every rotation.

As application of cutting fluid on the whole cutting tool is neither desired nor economical and environment friendly, so the first requirement is to calculate the net area where lubrication action is desired. As indicated by Li et al. (2019), the entire chip-tool contact region is divided into two regions, namely sticking zone and sliding zone. The sticking zone that occurs at the tool-tip influences built-up edge formation, alters chip morphology, determines cutting power, etc. There are several direct and indirect ways to determine the length of sticking zone; however, here an attempt has been made to geometrically estimate the length of such sticking zone for a rounded edge tool. Following the Lee and Shaffer's slip-line theory, it is assumed that the boundary of the plastic zone meets the rake surface at  $45^\circ$  angle (Toropov and Ko,

2003). Considering a continuous chip that is flowing over the flat rake surface of a rounded-edge cutting tool, the total tool-workpiece-chip contact length can be divided into three distinct segments (Fig. 4), namely  $L_1$ ,  $L_2$  and  $L_3$ .

In order to obtain the maximum contact length, it is necessary to visualize the contact scenario for the maximum uncut chip thickness condition (i.e. the end of up milling and beginning of down milling, where  $h_i = f_z$ ). Since workpiece material having thickness  $h_{min}$  fails to undergo shearing, the actual uncut chip thickness becomes  $a_1 = (f_z - h_{min})$ . Here it is assumed that shearing takes place along a concentrated plane, and finally a chip of thickness  $a_2 (> a_1)$  is obtained. This flowing chip maintains a plastic contact with the rake surface up to point-A. Accordingly, the length  $L_1$  (the contact length between the chip and straight portion of the rake surface) can be calculated as follows.

From the triangle  $\Delta OCA$ ,  $\angle OAC = 45^\circ$

$$\therefore \bar{AC} = \bar{OC} = a_2 \tag{1a}$$

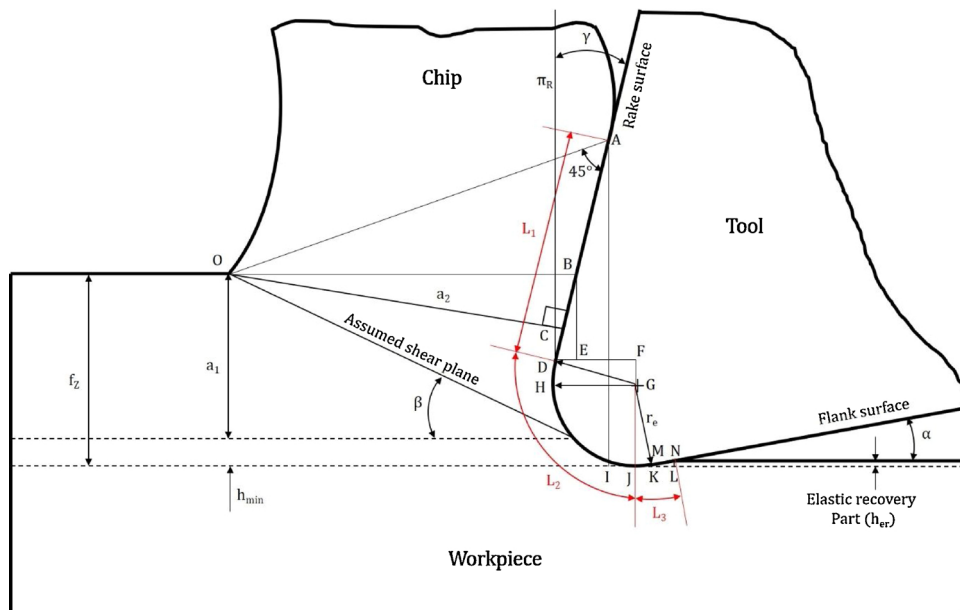


Fig. 4. Schematic representation of the tool-workpiece-chip contact zone, projected on a plane perpendicular to the tool axis.

Now consider the triangle  $\triangle OBC$ ,  $\angle BOC = \gamma$

$$\therefore \bar{BC} = a_2 \tan \gamma \quad (1b)$$

From  $\triangle DFG$ ,  $\angle GDF = \gamma$  and  $\bar{DG} = r_e$

$$\therefore \bar{BE} = f_z - r_e \sin \gamma - r_e \quad (1c)$$

From  $\triangle BDE$ ,  $\angle DBE = \gamma$

$$\therefore \bar{BD} = \frac{\bar{BE}}{\cos \gamma} = \frac{f_z - r_e(1 + \sin \gamma)}{\cos \gamma} \quad (1d)$$

$$\therefore \bar{CD} = (\bar{BD} - \bar{BC}) = \frac{f_z - r_e(1 + \sin \gamma)}{\cos \gamma} - (a_2 \tan \gamma) \quad (1e)$$

$$L_1 = \bar{AC} + \bar{CD} = a_2(1 - \tan \gamma) + \frac{f_z - r_e(1 + \sin \gamma)}{\cos \gamma} \quad (1f)$$

Segment-2 of length  $L_2$  evolves owing to the presence of comparatively large edge radius where intense rubbing takes place. A part of this segment converts into chip, while rest undergoes elastic-plastic deformation. As  $\angle DGH = \gamma$  and  $\bar{GH} = \bar{GD} = \bar{GJ} = r_e$ , so the arc length  $L_2$  can be expressed in terms of  $\gamma$  and  $r_e$ .

$$L_2 = r_e \left( \frac{\pi}{2} + \frac{\pi \gamma}{180} \right) \quad (2)$$

Segment-3 is the contact length between the flank surface of the tool and the workpiece material, and is influenced by elastic recovery of the concerned sample material. Thickness of the elastic recovery part ( $h_{er}$ ) can be calculated from the elastic strain ( $\epsilon_e$ ) of workpiece material, as given in Eq. 3. Since a layer of workpiece material having maximum thickness  $h_{min}$  undergoes elastic deformation, it can be safely assumed that  $h_{er} < h_{min}$ .

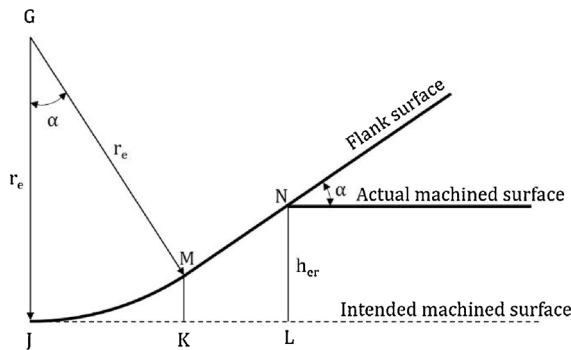
$$h_{er} = \epsilon_e h_{min} \quad (3)$$

However, based on the clearance angle of the cutting tool ( $\alpha$ ) and  $h_{er}$  value, two cases may arise, as shown in Fig. 5 as an extension of Fig. 4. In case-1, where  $h_{er} > r_e(1 - \cos \alpha)$  (i.e. the actual machined surface touches the flank surface outside the curved edge), the corresponding contact length  $L_3$  can be calculated as follows.

$$\bar{JM} = r_e \left( \frac{\pi \alpha}{180} \right) \quad (4a)$$

$$\bar{KM} = r_e(1 - \cos \alpha) \quad (4b)$$

$$\therefore \bar{MN} = \frac{h_{er} - r_e(1 - \cos \alpha)}{\sin \alpha} \quad (4c)$$



(a) Case-1:  $h_{er} \geq r_e(1 - \cos \alpha)$

$$L_3 = \bar{JM} + \bar{MN} = r_e \left( \frac{\pi \alpha}{180} \right) + \frac{h_{er} - r_e(1 - \cos \alpha)}{\sin \alpha} \quad (4d)$$

However, if  $h_{er} < r_e(1 - \cos \alpha)$  (i.e. the actual machined surface touches the flank surface within the curved portion of the edge), then the corresponding contact length  $L_3'$  can be calculated as follows. Therefore, either  $L_3$  or  $L_3'$  should be used to calculate entire contact length based on the  $\alpha$  and  $h_{er}$  values.

$$\alpha' = \cos^{-1} \left( 1 - \frac{h_{er}}{r_e} \right) \quad (5a)$$

$$L_3' = r_e \left( \frac{\pi \alpha'}{180} \right) = r_e \left( \frac{\pi}{180} \right) \left\{ \cos^{-1} \left( 1 - \frac{h_{er}}{r_e} \right) \right\} \quad (5b)$$

If  $h_{er} = r_e(1 - \cos \alpha)$ , then  $\alpha = \alpha'$  and  $L_3' = L_3$ ; and hence any one of Eqs. 4d and 5b can be utilized. In this work, workpiece material is PMMA, and for this material  $\epsilon_e \cong 0.05$  (Loock and Fleck, 2018). Accordingly,  $h_{er} < r_e(1 - \cos \alpha)$  condition is satisfied, and hence only  $L_3'$  is considered for further analysis.

Now, for a given axial depth ( $a_p$ ), length of the helical cutting edge ( $a_h$ ) which is in physical contact with the workpiece and is actually participating in material removal action can be calculated using helix angle ( $\Psi$ ).

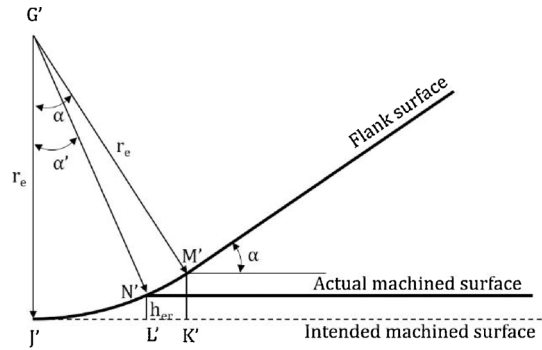
$$a_h = \frac{a_p}{\sin(90 - \Psi)} = \frac{a_p}{\cos \Psi} \quad (6)$$

Therefore, the net intended lubricated area ( $A_{lub}$ ) for each cutting edge where MQL oil must be applied in every rotation can be calculated from three contact lengths and cutting edge length, as follows.

$$A_{lub} = (L_1 + L_2 + L_3') a_h \quad (7)$$

### 3.3. MQL oil droplet density and size for specified nozzle-tool distance

To find out the number of MQL oil droplets required to completely lubricate the  $A_{lub}$  area, it is necessary to know the droplet size and droplet distribution for a predefined flow rate. In this investigation, two identical internally mixing nozzles are used for atomization purpose. The air-oil mixed jet, once comes out of the nozzle, experiences very low pressure (i.e. atmospheric pressure of 1 bar), and thus tends to flare. Accordingly, the diameter of the jet increases with the distance from the nozzle outlet. The impingement velocity of the oil droplets decreases with increase in nozzle-tool distance (NTD). Duchosal et al. (2015) highlighted that a higher impingement velocity increases the chances of post-impact rebounding and fragmentation of the droplets, rather than sticking to the tool surface. On the other hand, Maruda et al. (2016) showed that at a very large NTD, the droplets tend to



(b) Case-2:  $h_{er} \leq r_e(1 - \cos \alpha)$

Fig. 5. Schematic representation of the contact scenario between the flank surface of the tool and the machined surface of the workpiece where the actual machined surface touches the tool (a) outside and (b) within the rounded portion of the cutting edge.

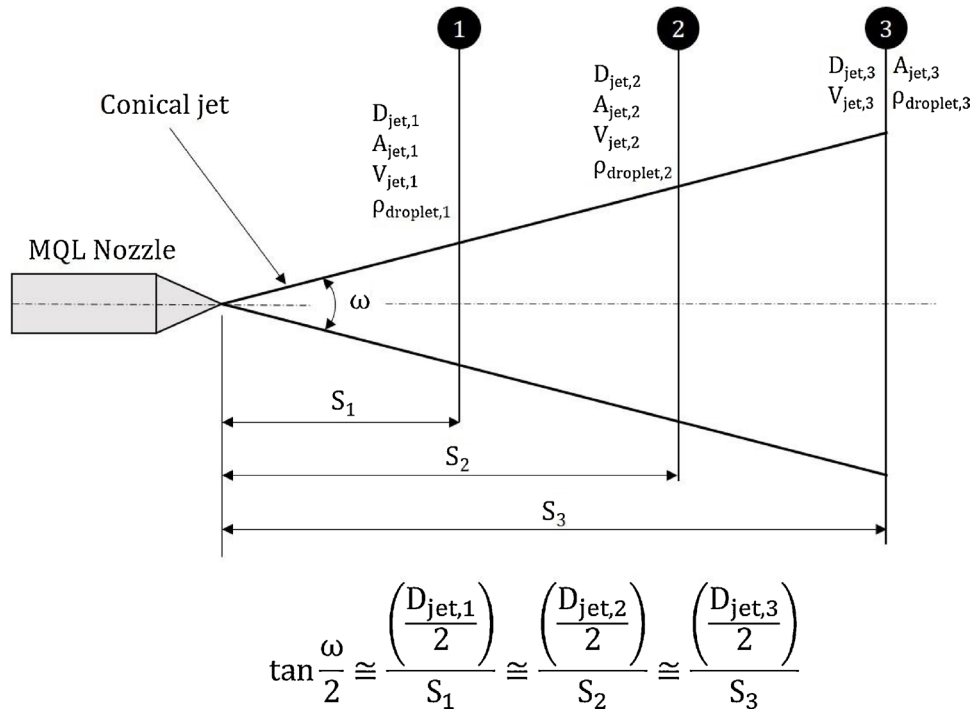
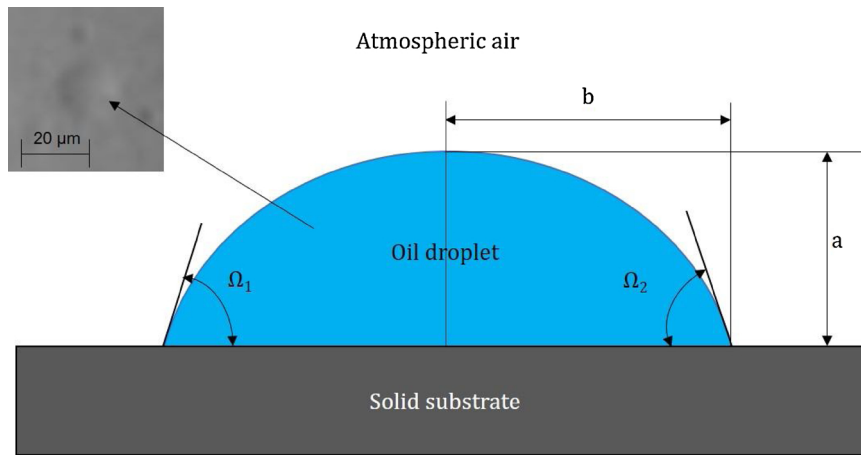


Fig. 6. Schematic representation of the conical shaped MQL jet for NTD in between 10 – 30 mm.

agglomerate as the jet velocity drops considerably. In this study, an uniform droplet size and homogeneous droplet distribution are obtained for an NTD range of 10–30 mm.

To further understand the flow pattern, a plate is kept perpendicular to the nozzle axis maintaining a distance of  $S_1 = 10\text{ mm}$ , and droplets are deposited on the plate (Fig. 6). The area where droplets are deposited is apparently a circle. The diameter of this circle is measured in five different directions and an average of them is found to be  $D_{jet,1} = 2.44\text{ mm}$ . The abovementioned steps are repeated for  $S_2 = 20\text{ mm}$  and  $S_3 = 30\text{ mm}$ , and the corresponding average diameters

are found to be  $D_{jet,2} = 4.84\text{ mm}$  and  $D_{jet,3} = 6.89\text{ mm}$ . Assuming the nozzle to be a point source, the apex angles can also be calculated from the corresponding  $S$  and  $D_{jet}$  values. The apex angles corresponding to NTD values of 10, 20 and 30 mm are  $\omega_1 = 13.9^\circ$ ,  $\omega_2 = 13.8^\circ$ , and  $\omega_3 = 13.1^\circ$ , respectively. Since  $\omega$  values are close, it can be assumed that  $S$  is proportional to  $D_{jet}$  in this range, and the jet has a conical shape (right cone). An average of  $\omega_1$ ,  $\omega_2$  and  $\omega_3$ , i.e.,  $\omega = 13.6^\circ$  is used for further analysis. Accordingly, the cross-sectional area of the jet ( $A_{jet}$ ) can be represented in terms of NTD and  $\omega$ , as follows.



$$\text{Contact angle } (\Omega) = \frac{\Omega_1 + \Omega_2}{2}$$

$$\text{Droplet volume} = \frac{1}{6} \pi a (3b^2 + a^2) \cong \frac{\pi}{2} ab^2 [\because a^2 \ll b^2]$$

$$\text{Wetting area, } A_{wet} = \pi b^2$$

Fig. 7. MQL oil droplet after impinging on the solid surface (a photograph of the droplet is shown in the inset).

$$A_{jet} = \pi S^2 \tan^2\left(\frac{\omega}{2}\right) \quad (8)$$

At higher NTD, the jet cross-sectional area is more, and thus the number of droplets striking the miniaturized cutting tool per unit time decreases. So in this work, all experiments are carried out for a constant NTD of 10 mm. To calculate the lubricant supply, a parameter called droplet density ( $\rho_{droplet}$ ) is introduced here, which is defined by the number of oil droplets impinge per second per unit area of a surface perpendicular to the jet axis. Owing to overlapping of the droplets, direct counting of droplet numbers deposited on a specified area is not practically feasible. Thus an indirect approach is considered here for estimating  $\rho_{droplet}$ . If volume flow rate of MQL oil is  $Q$  and volume of each droplet is  $V_{droplet}$ , then number of droplets produced per second ( $N_{droplet}$ ) from each of the two nozzles can be expressed as follows. Here it is assumed that each droplet has same volume.

$$N_{droplet} = \frac{Q}{2V_{droplet}} \quad (9)$$

When such droplets stay in air (i.e. flowing with the jet), they are assumed to remain spherical with a defined radius. So volume of each droplet ( $V_{droplet}$ ) can be calculated from the droplet radius ( $R_{droplet}$ ).

$$V_{droplet} = \frac{4}{3}\pi R_{droplet}^3 \quad (10)$$

On the other hand, if the MQL jet consisting of  $N_{droplet}$  droplets impinge a surface of area  $A_{jet}$  per second, then droplet density can be expressed as follows.

$$\rho_{droplet} = \frac{N_{droplet}}{A_{jet}} \quad (11)$$

In this investigation, the NTD is kept unchanged. So, Eq. 11 can be further modified to take the following form.

$$\rho_{droplet} = \frac{3Q}{8R_{droplet}^3 \left(\pi S \tan\frac{\omega}{2}\right)^2} \quad (12)$$

In Eq. 12,  $R_{droplet}$  is the only unknown parameter. It is not possible to measure droplet dimension when such droplets are flowing with jet. For the sake of measurement, droplets are allowed to impinge a TiAlN coated (matching with tool coating) solid surface kept perpendicular to the jet axis at 10 mm distance, and the diameter and height of the deposited droplets are measured. Schematic of such a droplet is shown in Fig. 7. An average contact angle of  $15.39^\circ$  indicates an adequate oil retention capability of TiAlN coated surface (Zhou et al., 2019). The average radius at the base and average height are found to be  $b = 7.3 \pm 0.51 \mu\text{m}$  and  $a = 0.82 \pm 0.06 \mu\text{m}$ , respectively. Accordingly, the volume of such deposited droplet can be calculated as follows.

$$V_{droplet-surface} = \frac{\pi}{2} ab^2 = 16.38 \mu\text{m}^3 \quad (13)$$

The droplet volume after impinging on the surface remains equal to the volume of the droplet entrained in the jet. Therefore, the radius of the droplet can be calculated equating Eq. 10 and Eq. 13. In this case,  $R_{droplet} = 2.54 \mu\text{m}$ . Now, for constant oil flow rate of  $Q = 1.67 \times 10^9 \mu\text{m}^3/\text{s}$ , NTD of  $S = 10,000 \mu\text{m}$  and apex angle of  $\omega = 13.6^\circ$ , the  $\rho_{droplet}$  can be calculated using Eq. 12.

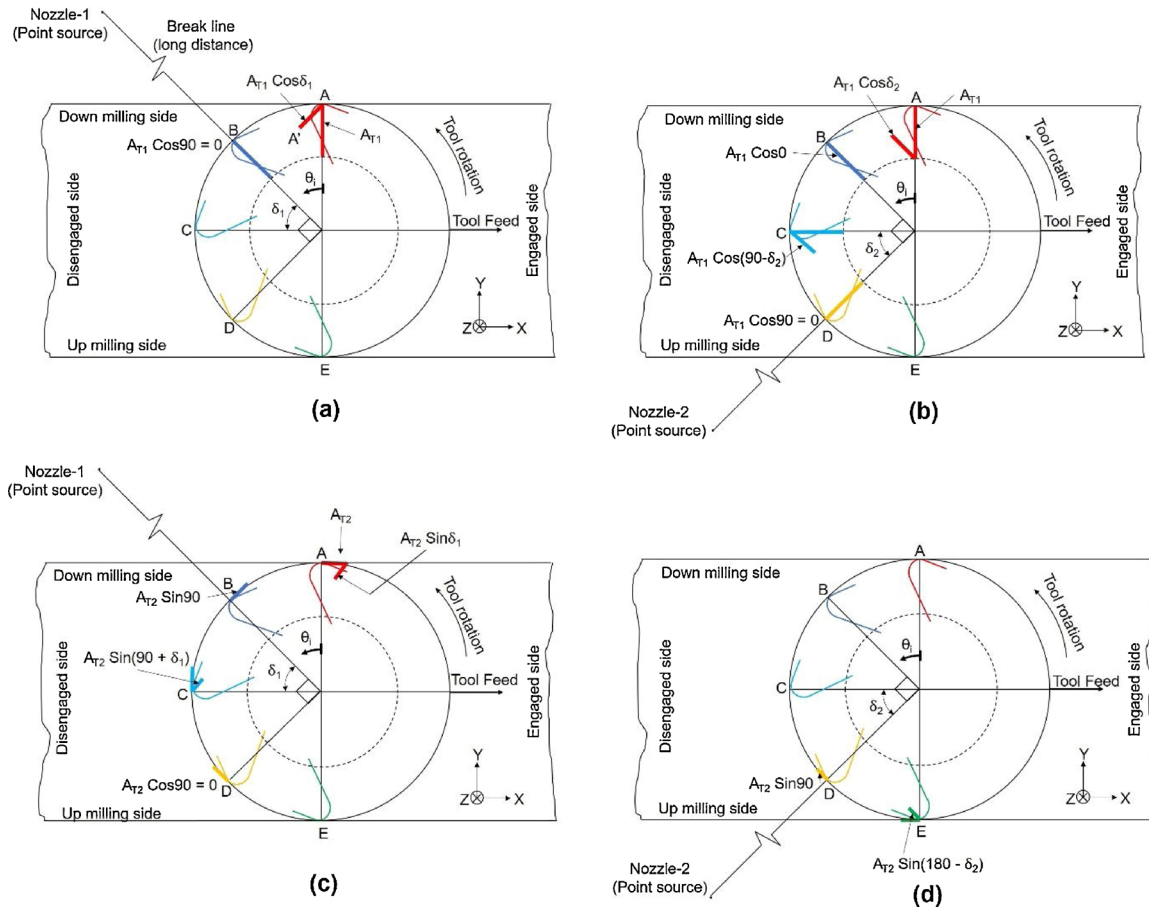


Fig. 8. MQL jet interaction scenario in the disengaged side for different locations (A-B-C-D-E) of the cutting edge for area (a)  $A_{T1}$  from nozzle-1, (b)  $A_{T1}$  from nozzle-2, (c)  $A_{T2}$  from nozzle-1, and (d)  $A_{T2}$  from nozzle-2.

$$\rho_{\text{droplet}} = 2.72 \mu\text{m}^{-2}\text{s}^{-1} \quad (14)$$

This indicates that, on an average, 2.72 droplets deposit per second per square micron area from each nozzle when this area is kept normal to jet axis at a distance of 10 mm. In this context, it is also imperative to find out wetting area ( $A_{\text{wet}}$ ), which is defined by the area on the solid surface that an oil droplet can lubricate or immerse. It is the circular area at the base of the droplet when it is deposited on the surface (Fig. 7), and can be calculated using average base radius  $b = 7.3 \mu\text{m}$ .

$$A_{\text{wet}} = \pi b^2 = 167.42 \mu\text{m}^2 \quad (15)$$

### 3.4. MQL oil droplet deposition on the cutting edge for specific nozzle setting angles

In general, the cutting oil cannot reach the tool-work-chip contact zone owing to immense contact pressure. In the case of full immersion slot milling using two flute cutter, each cutting edge remains in contact with the workpiece for only half of the time during one complete rotation. For rest half of the cycle, the same cutting edge remains exposed. Cutting oil can be easily deposited on the  $A_{\text{lub}}$  area during this disengagement period. The disengagement period ( $T_{\text{dis}}$ ), which is defined as the time for which each cutting edge remains separated from the workpiece in each revolution, can be expressed in terms of spindle speed ( $N$ ), as follows.

$$T_{\text{dis}} = \frac{60}{2N} \quad (16)$$

$T_{\text{dis}}$  is independent of the number of flutes present on the cutter body. However, it is inversely proportional to  $N$ , and hence, time available for wetting the  $A_{\text{lub}}$  area reduces at higher speed. Moreover, the area  $A_{\text{lub}}$  is not always perpendicular to the flowing MQL jet as the nozzles are set in a particular angle with respect to the tool axis. Additionally, the angular location of  $A_{\text{lub}}$  changes within this exposure time owing to the continuous rotation of the tool. For this,  $A_{\text{lub}}$  is perpendicular to the MQL jet only for an instance in the entire disengagement period. Thus, it is pertinent to interrelate the area and time of exposure for predefined nozzle positions. The lead of the tool helix is  $2721 \mu\text{m}$ , which is significantly larger than the axial depth of cut (maximum  $80 \mu\text{m}$ , Table 1). Hence, for the sake of simplicity, the cutting edge within the axial depth is assumed to be straight and inclined (rather than helical). Furthermore, the entire area  $A_{\text{lub}}$  is divided into two target areas ( $A_{T1}$  and  $A_{T2}$ ) in such a way that each of them experiences homogeneous exposure to the cutting fluid at any instance. With reference to Figs. 4 and 5, one target area ( $A_{T1}$ ) is parallel to the radial plane ( $\pi_R$ ) having width  $\bar{AI}$ . The other target area ( $A_{T2}$ ) is perpendicular to the radial plane having width ( $r_e + \bar{JL}$ ).

$$\bar{AI} = f_z + (L_1 \cos \gamma - \bar{BE}) = f_z + a_2 (\cos \gamma - \sin \gamma) \quad (17)$$

$$\bar{JL} = r_e \sin \alpha = \sqrt{h_{er}(2r_e - h_{er})} \quad (18)$$

As shown in Fig. 1, nozzles are inclined at a  $60^\circ$  angle in X-Z plane (i.e. normal to the cutting edge). Thus, length of target areas are determined by the axial depth of cut. This length is equal to the length of the helical cutting edge confined by the axial depth (i.e.  $a_h$  in Eq. 6). Accordingly, the surface areas of  $A_{T1}$  and  $A_{T2}$  can be expressed as follows.

$$A_{T1} = \frac{a_p}{\cos \psi} \{f_z + a_2 (\cos \gamma - \sin \gamma)\} \quad (19)$$

$$A_{T2} = \frac{a_p}{\cos \psi} \{r_e + \sqrt{h_{er}(2r_e - h_{er})}\} \quad (20)$$

Although the target areas do not change with rotational angle (or time) with respect to the X-Z plane, the same vary in the X-Y plane owing to continuous rotation of the cutting tool while the nozzles remain fixed. Such a scenario for each cutting edge in one rotation is

illustrated in Fig. 8 independently for two different nozzles for two different target areas. Since the NTD is significantly higher than the tool diameter, it can be safely assumed that  $\rho_{\text{droplet}}$  and  $R_{\text{droplet}}$  are invariable irrespective of the angular location of the target areas.

Nozzle-1 delivers cutting fluid from the down milling side making an angle  $\delta_1$  ( $0^\circ \leq \delta_1 \leq 90^\circ$ ) with the feed direction (Fig. 8a). The instantaneous angular location of a disengaged cutting edge is indicated by  $\theta_i$ , where  $\theta_i = 0^\circ$  indicates beginning of the disengagement and  $\theta_i = 180^\circ$  indicates completion of disengagement period for the concerned cutting edge. In this configuration, the area  $A_{T1}$  is exposed to the flowing jet of MQL fluid in between point-A ( $\theta_i = 0^\circ$ ) and point-B ( $\theta_i = 90^\circ - \delta_1$ ). At point-A, the area  $A_{T1}$  is not perpendicular to the MQL jet axis. Since  $\rho_{\text{droplet}}$  is calculated based on an area perpendicular to the jet axis (Fig. 6), it is necessary to consider a projected area for  $A_{T1}$  that is perpendicular to jet axis. Accordingly, projected area  $AA'$  having surface area  $A_{T1} \cos \delta_1$  appears. Therefore, all the MQL oil droplets within a portion of the jet having area  $A_{T1} \cos \delta_1$  deposit on the area  $A_{T1}$  at that instant. This projected area gradually decreases with the rotation of the edge from point-A to point-B. At point-B, it becomes zero as the area  $A_{T1}$  is parallel to the jet axis. After point-B, no more oil droplet can be deposited by nozzle-1 on  $A_{T1}$  as the concerned area moves opposite to the corresponding jet. Accordingly, the exposure time for area  $A_{T1}$  towards nozzle-1 ( $T_{\text{ex}}^{n1-A1}$ ) can be expressed as a function of total disengagement period ( $T_{\text{dis}}$ ) to the form of Eq. 21.

$$T_{\text{ex}}^{n1-A1} = \left( \frac{90 - \delta_1}{180} \right) T_{\text{dis}} \quad (21)$$

Since  $\rho_{\text{droplet}}$  denotes the number of MQL oil droplets deposited per unit area per second, the total number of useful droplets striking the area  $A_{T1}$  from nozzle-1 in each rotation can be obtained by integrating over the concerned exposure time, as given in Eq. 22.

$$\begin{aligned} N_{\text{useful-droplet}}^{n1-A1} &= \int_{\theta_i=0^\circ}^{\theta_i=(90^\circ-\delta_1)} \rho_{\text{droplet}} A_{T1} \cos \theta_i T_{\text{ex}}^{n1-A1} d\theta_i \\ &= \rho_{\text{droplet}} A_{T1} \sin(90 - \delta_1) \left( \frac{90 - \delta_1}{180} \right) \left( \frac{60}{2N} \right) \end{aligned} \quad (22)$$

Nozzle-2 is placed towards up milling side maintaining an angle of  $\delta_2$  ( $0^\circ \leq \delta_2 \leq 90^\circ$ ) with the feed vector (Fig. 8b). For this configuration,  $A_{T1}$  remains exposed to the flowing jet from point-A ( $\theta_i = 0^\circ$ ) to point-E ( $\theta_i = 90^\circ + \delta_2$ ). The corresponding exposure time ( $T_{\text{ex}}^{n2-A1}$ ) can be expressed as given in Eq. 23. Total number of useful droplets striking the area  $A_{T1}$  from nozzle-2 in each rotation of the tool can be calculated as follows.

$$T_{\text{ex}}^{n2-A1} = \left( \frac{90 + \delta_2}{180} \right) T_{\text{dis}} \quad (23)$$

$$\begin{aligned} N_{\text{useful-droplet}}^{n2-A1} &= \int_{\theta_i=0^\circ}^{\theta_i=(90^\circ+\delta_2)} \rho_{\text{droplet}} A_{T1} \cos(\theta_i - \delta_2) T_{\text{ex}}^{n2-A1} d\theta_i \\ &= \rho_{\text{droplet}} A_{T1} (1 + \sin \delta_2) \left( \frac{90 + \delta_2}{180} \right) \left( \frac{60}{2N} \right) \end{aligned} \quad (24)$$

MQL oil droplet deposition scenario on another target area  $A_{T2}$  can also be considered in similar way without changing the nozzle positions. Fig. 8c shows the exposure pattern for area  $A_{T2}$  towards nozzle-1. In this configuration,  $A_{T2}$  is exposed to flowing jet in between point-A ( $\theta_i = 0^\circ$ ) and point-D ( $\theta_i = 180^\circ - \delta_1$ ). The corresponding exposure time ( $T_{\text{ex}}^{n1-A2}$ ) and the number of useful droplets ( $N_{\text{useful-droplet}}^{n1-A2}$ ) can be estimated as follows.

$$T_{\text{ex}}^{n1-A2} = \left( \frac{180 - \delta_1}{180} \right) T_{\text{dis}} \quad (25)$$

$$N_{\text{useful-droplet}}^{n1-A2} = \int_{\theta_i=0^\circ}^{\theta_i=(180^\circ-\delta_1)} \rho_{\text{droplet}} A_{T2} \sin(\delta_1 + \theta_i) T_{\text{ex}}^{n1-A2} d\theta_i$$

$$= \rho_{\text{droplet}} A_{T2} (1 + \cos \delta_1) \left( \frac{180 - \delta_1}{180} \right) \left( \frac{60}{2N} \right) \quad (26)$$

Similarly, the area  $A_{T2}$  remains exposed to MQL jet from nozzle-2 (Fig. 8d) in between point-D ( $\theta_i = 90^\circ + \delta_2$ ) to point-E ( $\theta_i = 180^\circ$ ). Thus, the concerned exposure time and number of useful droplets can be expressed as follows.

$$T_{\text{ex}}^{n2-A2} = \left( \frac{90 - \delta_2}{180} \right) T_{\text{dis}} \quad (27)$$

$$N_{\text{useful-droplet}}^{n2-A2} = \int_{\theta_i=90^\circ+\delta_2}^{\theta_i=180^\circ} \rho_{\text{droplet}} A_{T2} \sin(\theta_i - \delta_2) T_{\text{ex}}^{n2-A2} d\theta_i$$

$$= \rho_{\text{droplet}} A_{T2} \cos \delta_2 \left( \frac{90 - \delta_2}{180} \right) \left( \frac{60}{2N} \right) \quad (28)$$

Although  $\delta_1$  and  $\delta_2$  has a theoretical range of  $0^\circ \leq \delta_1, \delta_2 \leq 90^\circ$ , judicious selection of these two angles are necessary to achieve a better exposure. Both the angles  $\delta_1$  and  $\delta_2$  simultaneously cannot be zero as it undesirably changes the NTD and nozzle orientation in X-Z plane. Furthermore, if both are made  $90^\circ$ , then oil flow from one nozzle can oppose the other one. This can also change the jet characteristics and alter the direction of flow of the droplets. These angles are also limited by the geometry of the tool and number of flutes. With reference to Fig. 2a, if  $\delta_2$  becomes more than  $48^\circ$  then the corresponding exposure can get affected owing to the restriction imposed by the secondary flank surface of the other cutting edge. Thus, in this work, experiments are carried out for  $\delta_1 = \delta_2 = 45^\circ$ .

#### 4. Results and discussion

End milling inherently produces discontinuous chips as every cutting edge engages and disengages with the workpiece in each rotation. During the engagement period the uncut chip thickness gradually increases in up milling side and then decreases in down milling side; and thus the thickness of the chip is also not constant throughout its length. Since the length  $L_1$  depends on chip thickness (Eq. 1f), it is necessary to find out the maximum thickness of the chip ( $a_2$ ) that occurs at the end of up milling phase for an edge (at  $a_1 = f_z - h_{\text{min}}$ ). For measurement purpose, chips are observed under the SEM and thickness values are measured by properly orienting the sample holder. However, the chip under observation might be a broken chip. Thus, its highest thickness may not correspond to the actual maximum chip thickness. A complete discontinuous chip generated by a cutting edge in a rotation during full immersion slot milling ideally has the maximum thickness at only one intermediate point, while left and right sides of this point have gradually decreasing thicknesses. Accordingly, if the thickness of a complete chip is measured at successive points along its length, and the same is plotted against the length of the chip, then an inverted U-shaped curve is obvious (Fig. 9b). The zenith of such curve gives the intended maximum chip thickness ( $a_2$ ). The number of measurements is kept reasonably high (at least 25 points) with closer points surrounding the maximum value in order to obtain a smooth curve avoiding local fluctuations. Uniformity in chip thickness among all the collected chips for each slot is ensured by the absence of phase difference, as discussed later in this section.

As shown in Fig. 9c, the maximum chip thickness ( $a_2$ ) is found to vary with speed and cutting environment. However, appreciable variation of  $a_2$  with axial depth of cut is not observed as axial depth is significantly higher than the edge radius ( $a_p \gg r_e$ ). Decreasing tendency of chip thickness with the increase in speed during macro-scale high

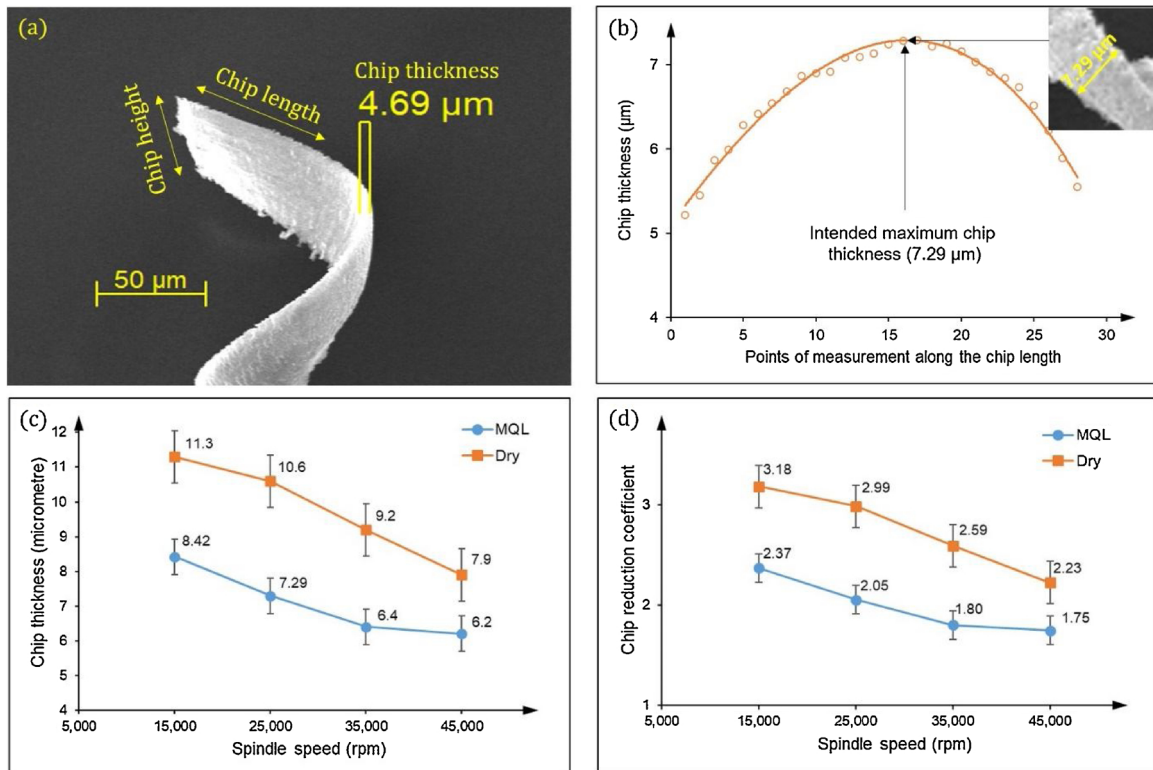


Fig. 9. (a) Typical SEM image of a part of the chip showing the directions of height, length and thickness, (b) inverted U-shaped curve obtained by plotting measured thickness along chip length, the zenith of which gives the intended maximum chip thickness (a magnified view of the middle portion of the chip is also shown in inset), (c) variation of chip thickness with speed, and (d) corresponding variation of chip reduction coefficient (CRC).

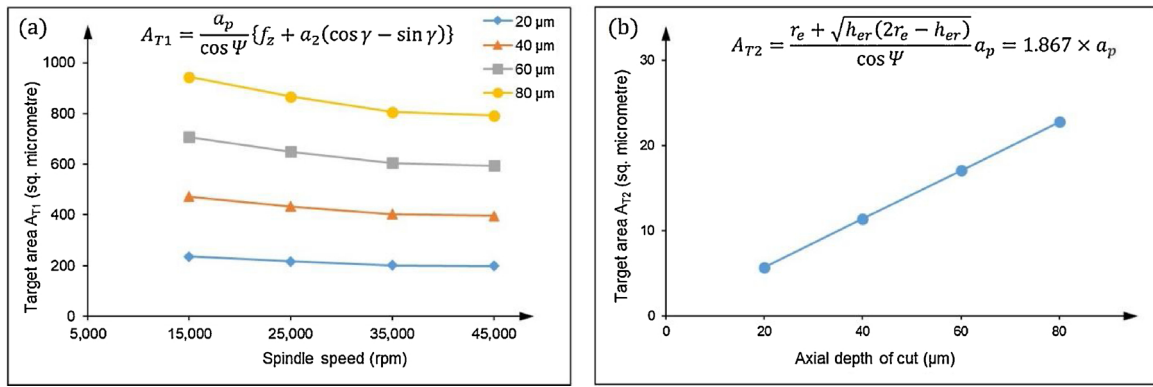


Fig. 10. Variations of target areas  $A_{T1}$  and  $A_{T2}$  with speed and axial depth for MQL assisted cutting.

speed turning was also observed by Sutter and List (2013). A parameter called chip reduction coefficient (CRC,  $\zeta$ ) is introduced which is defined by the ratio between chip thickness ( $a_2$ ) and uncut chip thickness ( $a_1$ ). CRC can be calculated from the known value of  $a_1$  and measured value of  $a_2$ . As the feed and cutting tool is unchanged, so  $a_1 = (f_z - h_{min}) = (4 - 0.45) = 3.55 \mu\text{m}$  for all the cases, whereas  $a_2$  value changes slightly. The CRC value gives an idea about the degree of deformation of the chip owing to shearing. As shown in Fig. 9d,  $\zeta > 1$  in all cases indicates a positive cutting strain as the chips are getting thickened.  $\zeta$  also decreases with spindle speed. For all the speeds,  $\zeta$  is higher in dry cutting as compared to MQL assisted cutting. At 15,000 rpm, the  $\zeta$  value for MQL assisted cutting is about 34 % smaller than that for dry cutting. This difference reduces to 27 % at 45,000 rpm. Such a reduction is possibly owing to the deficiency in lubrication at higher speeds regardless of the axial depth, as discussed in the

following passages. For a constant uncut chip thickness (as  $f_z$  is constant), a decreasing trend of  $\zeta$  with speed also indicates that the intended lubricated area (Eq. 7) reduces with the increase in speed.

Since the concept of target areas is useful in estimating MQL oil droplet delivery scenario, such areas have no significance in dry cutting. The target area  $A_{T1}$  depends on axial depth as well as chip thickness, which, in turn, relies on spindle speed. Owing to the existence of proportional relationship (Eq. 19), area  $A_{T1}$  is more at higher axial depth (Fig. 10a). The same area decreases with an increase in speed following the corresponding variation of chip thickness. Unlike area  $A_{T1}$ , the target area  $A_{T2}$  is depends only on the axial depth (Fig. 10b). Although the area  $A_{lub}$  reduces with speed, the time  $T_{dis}$  and area  $A_{T1}$  both decrease with speed. Hence it is necessary to consider lubrication demand and supply relationship for a given set of process parameters. Total number of droplets that are striking each cutting edge

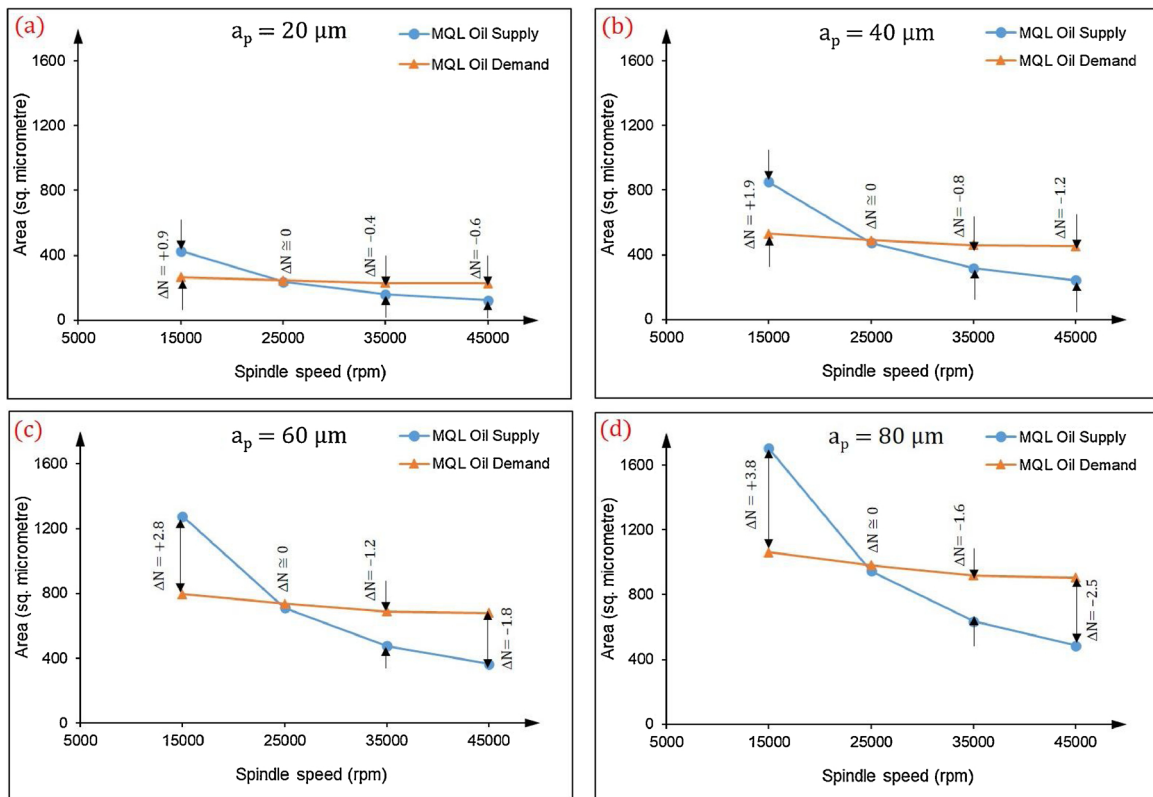


Fig. 11. Cutting oil demand and supply scenarios for varying speeds in MQL assisted micromilling at an axial depth of (a) 20  $\mu\text{m}$ , (b) 40  $\mu\text{m}$ , (c) 60  $\mu\text{m}$ , and (d) 80  $\mu\text{m}$ .

at a particular speed and axial depth can be calculated by adding all four  $N_{useful-droplet}$  elements. This number may not necessarily be an integer as a fraction indicates that only a portion of a droplet is situated within the required  $A_{lub}$  zone. Thus, total area covered (or lubricated) under this supplied oil can be calculated from total number of supplied droplets and the wetting area (Eq. 15). Based on this demand and supply scenario for each combination of speed and axial depth, three possible cases arise, as follows.

$$Abundant\ Supply: A_{lub} < (N_{useful-droplet}^{n1-A1} + N_{useful-droplet}^{n2-A1} + N_{useful-droplet}^{n1-A2} + N_{useful-droplet}^{n2-A2})A_{wet} \quad (29a)$$

$$Adequate\ Supply: A_{lub} = (N_{useful-droplet}^{n1-A1} + N_{useful-droplet}^{n2-A1} + N_{useful-droplet}^{n1-A2} + N_{useful-droplet}^{n2-A2})A_{wet} \quad (29b)$$

$$Deficient\ Supply: A_{lub} > (N_{useful-droplet}^{n1-A1} + N_{useful-droplet}^{n2-A1} + N_{useful-droplet}^{n1-A2} + N_{useful-droplet}^{n2-A2})A_{wet} \quad (29c)$$

The nature of variation of demand and supply curves with spindle speed is similar for all axial depths, as shown in Fig. 11. For a particular

speed, changes in axial depth do not lead to any perceptible change in droplet demand and supply scenario since both the target areas and the intended lubricated areas proportionally increase with axial depth. On the other hand, the MQL droplet supply is significantly higher than the demand at 15,000 rpm spindle speed for all axial depths. As speed increases, the supply gradually drops below the demand level. At 25,000 rpm speed, the supply becomes marginally lower than the corresponding demand. For all higher speed values, this difference between demand and supply increases. This is owing to the fact that the available time to lubricate the intended surface decreases with speed. Thus, the effect of cutting speed is more pronounced as compared to axial depth in high speed micromilling. The difference between demand and supply is measured in terms of droplet deficiency or abundance ( $\Delta N$ ) per cutting edge per revolution, as expressed below.

$$\Delta N = \frac{(N_{useful-droplet}^{n1-A1} + N_{useful-droplet}^{n2-A1} + N_{useful-droplet}^{n1-A2} + N_{useful-droplet}^{n2-A2})A_{wet} - A_{lub}}{A_{wet}} \quad (30)$$

Accordingly,  $\Delta N > 0$  indicates abundance in supply,  $\Delta N = 0$

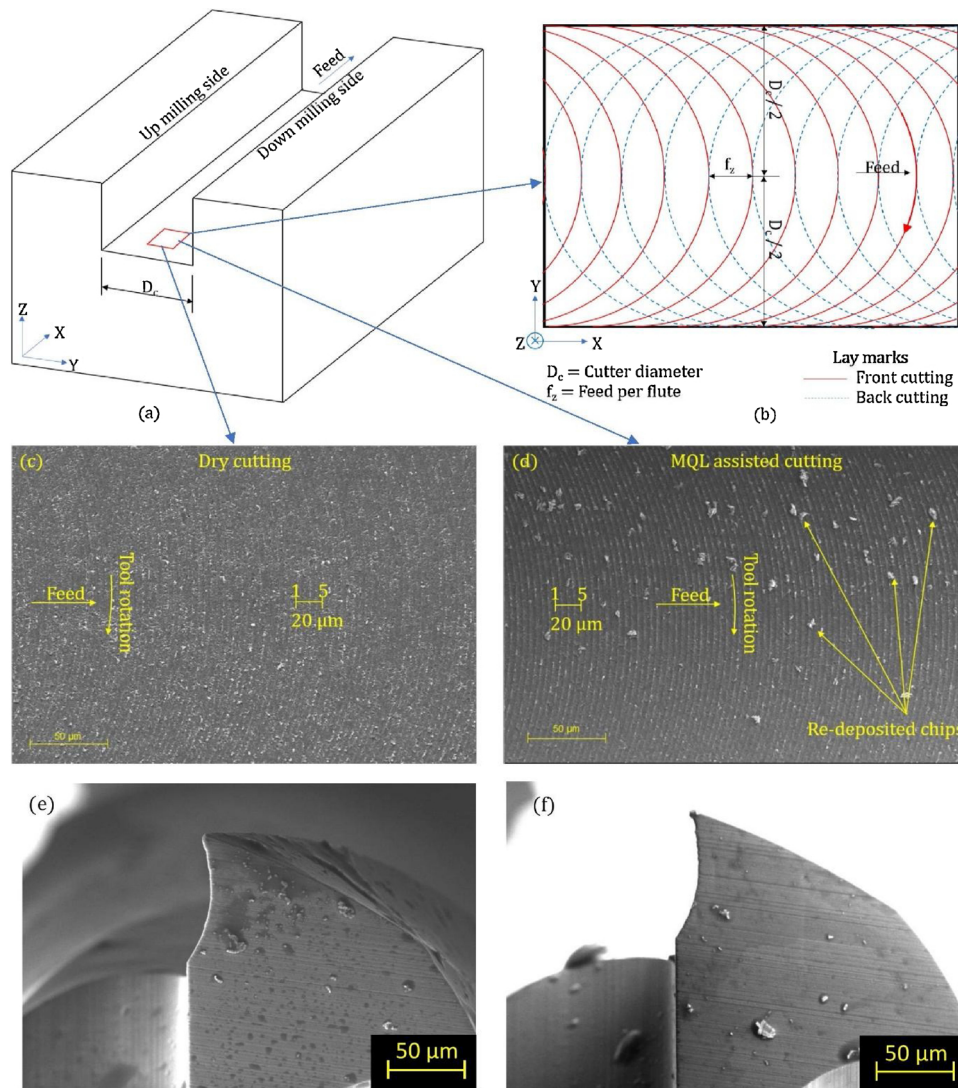


Fig. 12. Schematic illustrations of the (a) generated surfaces in full immersion slot milling, and (b) bottom surface of the slot consisting of front cutting and back cutting lay marks; typical SEM images of the bottom surface of the as-machined slot obtained in (c) dry micromilling and (d) MQL assisted micromilling; and corresponding tool condition in (e) dry micromilling and (f) MQL assisted cutting for  $N = 35,000$  rpm,  $f_z = 4 \mu\text{m}/\text{flute}$ ,  $a_p = 40 \mu\text{m}$ .

indicates adequate supply, and  $\Delta N < 0$  indicates deficiency in supply. For each spindle speed, the magnitude of  $\Delta N$  varies considerably with axial depth. Thus it can be inferred that, although the deficient condition arises mainly due to the spindle speed, the degree of deficiency in oil supply depends on axial depth. Accordingly, the oil flow rate is required to increase proportionally with the increase in axial depth. Impacts of abundant and deficient lubrication supply on surface characteristics are studied further. Presence of lay marks on the as-machined bottom-surface (Fig. 12a) is one characteristics feature of micromilling process. Ideally, every cutting edge in each rotation leaves behind a tiny portion of uncut material on the bottom surface that ultimately reflect as lay mark. Ideally, the lay marks are also uniformly distributed and the spacing between two successive lay marks is equal to feed per flute set during micromilling operation (Fig. 12b). As typically shown in Fig. 12c and d, a 20  $\mu\text{m}$  line consists of exactly 5 peaks. This matches the given feed ( $f_z = 4 \mu\text{m}/\text{flute}$ ). Moreover, the lay marks are uniformly distributed over the entire surface. Hence, it can be inferred that material removal took place by each cutting edge in every rotation. No appreciable difference in lay mark distribution is observed with the variation in axial depth and speed and also with the changes in cutting environment.

Furthermore, the lay marks are oriented along the trajectory of the engaged cutting edge (revealed by the convex shape with the feed direction). As indicated by Melkote and Thangaraj (1994), the texture of the bottom surface in end-milling is usually generated by the superimposition of the front cutting by the engaged cutting edge and back cutting by the trailing cutting edge (Fig. 12b). Lay marks generated by the back cutting have concave shape with respect to the feed vector. Franco et al. (2008) also concluded that back cutting can reduce the height of the lay marks generated by the front cutting; however, usually at the cost of surface smearing. Additionally, back cutting is promoted by the phase difference between the front cutting and back cutting. In this investigation, no evidence of back cutting is detected in any case, that rules out the existence of phase difference between two cutting edges even at high depth of cut and high velocity. Absence of back cutting can be attributed to a very low cutting force in micromilling of PMMA samples. No galling and seizure wear is also detected on the bottom surface. The absence of back cutting along with the uniform and consistent lay marks ensures that all the chips collected for each slot have uniform thickness, as shown earlier in Fig. 9.

Typical bottom surfaces of the as-machined slot obtained in dry and MQL assisted cutting along with the corresponding tool condition are also shown in Fig. 12. Application of cutting fluid has no significant influence on breakage of the cutting tool. In fact, no breakage of tool-tip or edge is noticed even in dry cutting. Very low cutting force that develops during micromilling of a soft material like PMMA is not enough to induce tool breakage. However, a few micro-chips are found to remain loosely adhered on various faces of cutting tool. Traces of brittle

fracture are observed on the as-machined dry cut bottom-surface. It may be noted that PMMA substrates typically have a very low fracture toughness, in the range of  $0.87 - 1.20 \text{ MPa}\sqrt{\text{m}}$  (Choi and Salem, 1993). Thus, it is susceptible to fracture.

Dry cut bottom surfaces are mostly free from re-deposited chips. On the contrary, the tendency of re-deposition of micro-chips is higher in the case of MQL assisted micromilling. This is attributed to the fact that the high velocity jet of the cutting fluid removes the chips that are sticking to the cutting tool after the engagement period in each rotation. This helps in cleaning the tool in each rotation, but at the same time, a portion of such removed chips are deposited on the as-machined surface behind the cutting tool. The nozzle orientation in the X-Z plane (Fig. 1a) increases the tendency of re-depositing the chips within the slot surface after sweeping the adhered chips from the tool. This can be considered as a drawback of MQL assisted micromilling. A similar observation was also highlighted by Thepsonthi et al. (2009). It is also observed that the number of re-deposited chips present on the bottom surface is more at higher axial depth. This is possibly owing to fact that the volume of chips adhered within the gullet of the cutting tool increases with an increase in axial depth. In addition, low process temperature prevents welding of such chips with the machined surface. No sign of micro-cutting or scratch marks caused by the re-deposited chips on the as-machined surface is also detected. It indicates that re-deposition occurred only after the tool passed over the concerned surface.

As indicated by Muñoz-Escalona and Maropoulos (2015), feed per flute and tool geometry (particularly edge radius and end cutting edge angle) are crucial parameters that determine surface roughness. In the current work, since feed and tool are kept unchanged, a large variation in surface roughness is not expected. As shown in Fig. 13a,  $R_a$  value for dry cutting typically increases with speed regardless of axial depth. However, for a constant speed, no appreciable change in  $R_a$  value with axial depth is detected in dry cutting. The percentage difference in  $R_a$  value (i.e.  $\Delta R_a$ ) between dry and MQL assisted cutting is also shown in Fig. 13b. A positive value of  $\Delta R_a$  in every occasion indicates that MQL assisted micromilling gives lower average roughness as compared to the corresponding cases in dry cutting. Thus, the higher is the value of  $\Delta R_a$  ( $0\% \leq \Delta R_a \leq 100\%$ ), the better is the capability of lubricant in reducing surface roughness. At 15,000 rpm, abundant lubricant is applied on the cutting edges regardless of the axial depth. Accordingly,  $\Delta R_a$  is highest at 15,000 rpm among all the speeds investigated here. With increase in speed, the  $\Delta R_a$  value gradually drops. However, there is not much difference in  $\Delta R_a$  value between 15,000 rpm and 25,000 rpm. This is possibly because of the fact that, although deficient lubrication condition exists at 25,000 rpm, the degree of deficiency is very low (i.e.  $\Delta N \cong 0$  as shown in Fig. 11). With further increase in speed, the impact of lubricant deficiency can be clearly observed. Since  $\Delta N$  also increases with axial depth of cut, a decreasing trend of  $\Delta R_a$  is natural. This is perceptible particularly at higher speed and higher axial depth as the

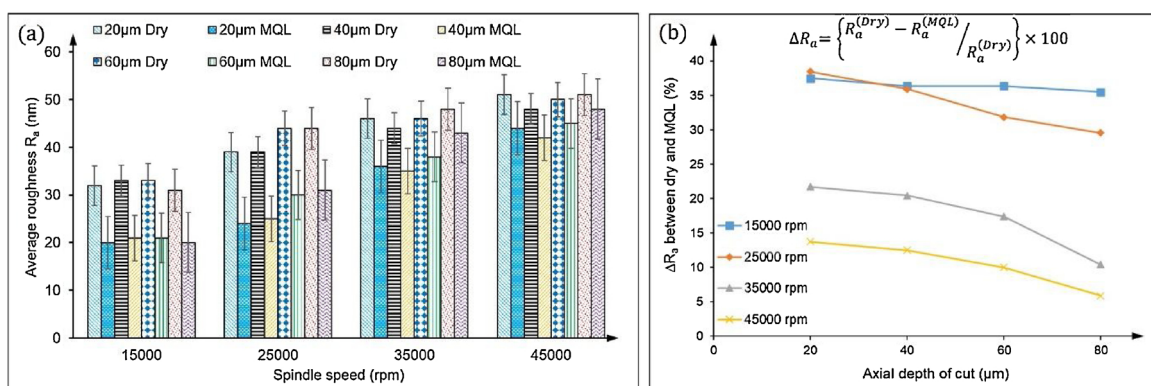


Fig. 13. Variation of average surface roughness for dry and MQL assisted cutting under varying speed and axial depth.

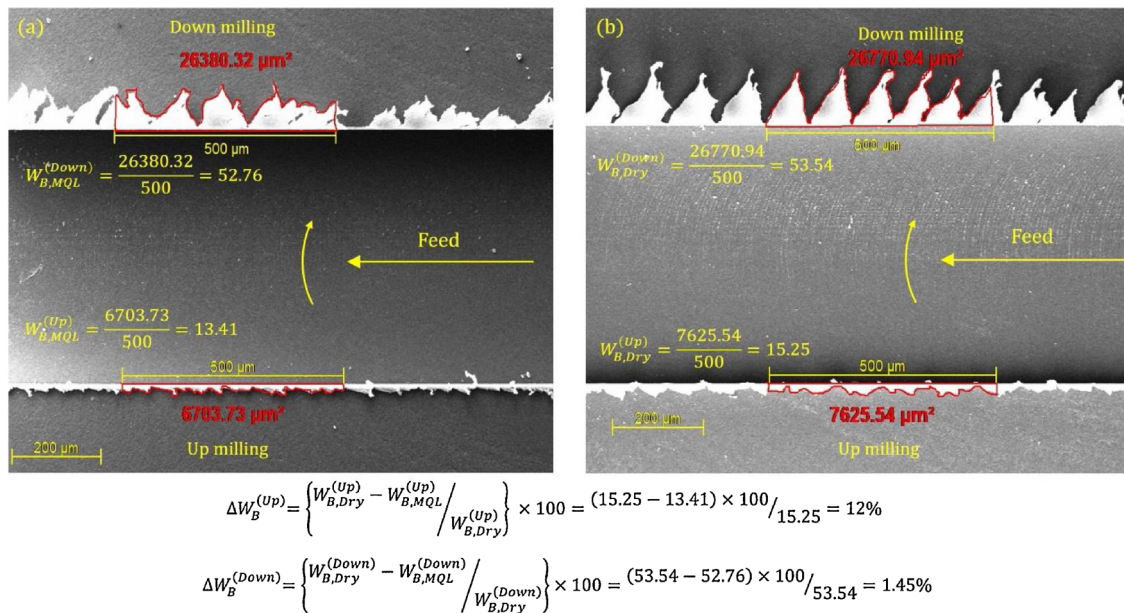


Fig. 14. Average top-burr width measurement procedure from the actual area of the burr that generates in (a) MQL assisted cutting, and (b) dry cutting at 45,000 rpm speed and 60 μm axial depth.

degree of deficiency can be strongly felt on such condition. Thus it can be inferred that it is not only the lubrication deficient condition but also the degree of deficiency can strongly influence the machined surface quality.

To explore the influences of abundant and deficient lubrication on burr formation, the average top-burr width ( $W_B$ ) is considered as the indicative parameter. Top-burrs, in both up and down milling sides, are mainly Poisson burrs that form owing to the lateral deformation of workpiece material instead of proper shearing (Chern and Dornfeld, 1996). Burrs are observed under SEM prior to ultrasonic cleaning of the slots as such cleaning also acts as a deburring method (Yeo et al., 1997). Since top-burr has non-uniform width, an average width is measured from the surface area, as described by Medeossi et al. (2018). Here the irregular shaped burrs within a sample length is projected to a rectangle having same area and sample length. As shown in Fig. 14, the actual burr area for a slot of length 0.5 mm is measured, and the same is divided by the corresponding length to obtain the  $W_B$ . The percentage difference in top-burr width ( $\Delta W_B$ ) between dry and MQL assisted cutting are plotted separately for up and down milling burrs.

As the nozzles are equispaced (i.e.  $\delta_1 = \delta_2 = 45^\circ$ ), so both up and down milling burrs experience similar exposure of MQL jet. As usual,

down milling is found to generate more burr as compared to up milling (Wu et al., 2017). Moreover, burr width typically decreases with an increase in speed. Irrespective of the speed and axial depth, a positive value of  $\Delta W_B$  indicates that dry milling generates more top-burr as compared to MQL assisted cutting. In up milling side (Fig. 15a),  $\Delta W_B$  is higher at lower speed for every axial depths. A higher  $\Delta W_B$  indicates that burr width in MQL assisted micromilling is substantially lower than that for dry cutting. Since abundant cutting fluid is delivered at 15,000 rpm for all axial depths, it can be inferred that abundance in lubrication can effectively reduce top-burr width. At higher axial depth,  $\Delta W_B$  steeply decreases with increase in speed; while an opposite nature can be observed at lower axial depth. Since the number of deficient oil droplets ( $\Delta N$ ) is more at higher axial depth, the degree of deficiency towards  $\Delta W_B$  is more pronounced at higher axial depth. Although the nature of variation of  $\Delta W_B$  in down milling side is similar to that observed for up milling side, the values of  $\Delta W_B$  for down milling is somewhat less (Fig. 15b). When oil droplets are deposited on the cutting tool during disengagement period, the lubrication effect can be better visualized in the up milling side burrs as it occurs just after the droplet deposition. The bulk amount of deposited lubricant flows away with chip in the up milling quarter-cycle, and the down milling runs in

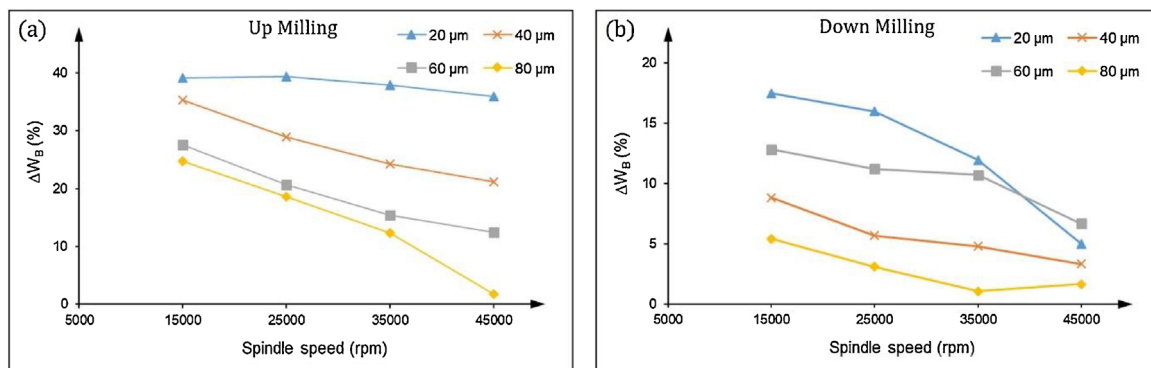


Fig. 15. Variation of  $\Delta W_B$  between dry and MQL assisted micromilling for (a) up, and (b) down milling.

a lubricant deficient condition. Thus, the lubrication has negligible influence on the down milling side top-burr.

## 5. Conclusions

This investigation attempts to explore the interaction between flowing droplets of cutting oil and rotating micro-end mill to find out whether a given MQL oil supply is adequate or not during MQL assisted high speed micromilling. An analytical model is first developed to calculate the intended area of lubrication for each cutting edge. The actual chip-tool and tool-workpiece contact lengths are calculated based on the tool geometry and workpiece material properties. Thereafter, the number of oil droplets striking per unit area per unit time is estimated from the characteristics of MQL jet and oil droplets. An interrelationship between the oil droplet demand and the corresponding supply is then analytically established to evaluate the role of spindle speed and axial depth of cut in determining abundant, adequate and deficient oil supply conditions. Validation is also carried out through micromilling experiments on PMMA samples with varying speeds and axial depths but for constant MQL oil flow rate. Based on the analysis of the results, following conclusions are made.

- 1 Similar to uncut chip thickness, the thickness of a particular chip is also not constant. A procedure is proposed to find out the maximum chip thickness that occurs at the middle of the slot in full immersion micromilling. When axial depth is significantly larger than edge radius, the chip thickness remains unaffected by the axial depth. However, chip thickness decreases with the increase in spindle speed regardless of the axial depth. The chip reduction coefficient (CRC) at 15,000 rpm spindle speed is 3.18 and 2.37 for dry and MQL assisted cutting, respectively. The respective CRC value reduces to 2.23 and 1.75 at 45,000 rpm.
- 2 Since the cross-sectional area of MQL jet is substantially higher than the tool diameter, any increase in axial depth leads to a proportional increase in the exposed area that receives oil droplets. So higher axial depth does not lead to lubricant deficient condition as long as the speed is reasonably low. However, deficient lubrication condition may occur if speed exceeds certain limit, even at low axial depth. For this investigation condition, 6 mL/hr MQL oil flow rate is found abundant for 15,000 rpm spindle speed, adequate for 25,000 rpm, but deficient for higher speeds.
- 3 In micromilling of a soft material like PMMA, only front cutting lay marks can be detected regardless of the cutting environment and process parameters. Such lay marks are homogeneous and uniformly distributed throughout the bottom surface. Distance between two adjacent lay marks (4  $\mu\text{m}$ ), when measured at the middle of the slot, also matches the given feed per flute (4  $\mu\text{m}/\text{flute}$ ). Dry cut bottom-surfaces are affected by brittle fracture. Micro-fracturing of the bottom-surface can be prevented by applying MQL cutting oil. However, application of MQL increases the tendency of re-deposition of micro-chips.
- 4 Proper lubrication can effectively reduce the bottom surface roughness ( $R_a$ ). Not only the lubrication deficient condition but also the degree of deficiency has influence on  $R_a$  value. Irrespective of axial depth, the  $R_a$  value for dry cutting at 15,000 rpm is about 37 % higher than that for MQL assisted cutting. This difference is less for higher speeds, and the same also reduces with axial depth.
- 5 Deficient supply of MQL oil can undesirably increase the top-burr width in up milling side. For a constant oil flow rate, the oil deficient area increases proportionally with the axial depth. Accordingly, the influence of deficient oil supply on the top-burr width is clearly noticeable at higher axial depth. The up milling side top-burr width in MQL assisted cutting in well-lubricated condition (15,000 rpm) is about 40 % lower than that for dry cutting.
- 6 In full immersion slot milling, an up milling quarter-cycle is followed by a down milling quarter-cycle. The bulk amount of

deposited lubricant is utilized in the up milling quarter-cycle, and down milling runs in lubricant deficient condition. Hence, the effect of lubricant in reducing top-burr in down milling side is not perceptible. Accordingly, the down milling top-burr width in well-lubricated condition in MQL assisted cutting is just 17 % lower than that in dry cutting.

## CRedit authorship contribution statement

**Suman Saha:** Problem definition execution of the work primary analysis, Writing first draft. **Sankha Deb:** Providing facility and supervision. **Partha Pratim Bandyopadhyay:** Problem definition supervision criticism monitoring, Writing - review & editing.

## Declaration of Competing Interest

The authors declare that they have no known competing financial interests or personal relationships that could have appeared to influence the work reported in this paper.

## References

- Abellan-Nebot, J.V., Rogero, M.O., 2019. Sustainable machining of molds for tile industry by minimum quantity lubrication. *J. Cleaner Prod.* 240, 118082. <https://doi.org/10.1016/j.jclepro.2019.118082>.
- Baburaj, M., Ghosh, A., Shunmugam, M., 2017. Study of micro ball end mill geometry and measurement of cutting edge radius. *Precis. Eng.* 48, 9–17. <https://doi.org/10.1016/j.precisioneng.2016.10.008>.
- Bruschi, S., Tristo, G., Rysava, Z., Bariani, P., Umbrello, D., Chiffre, L.D., 2016. Environmentally clean micromilling of electron beam melted Ti6Al4V. *J. Cleaner Prod.* 133, 932–941. <https://doi.org/10.1016/j.jclepro.2016.06.035>.
- Chern, G.-L., Dornfeld, D.A., 1996. Burr/Breakout model development and experimental verification. *J. Eng. Mater. Technol.* 118, 201–206. <https://doi.org/10.1115/1.2804887>.
- Choi, S., Salem, J., 1993. Fracture toughness of PMMA as measured with indentation cracks. *J. Mater. Res.* 8, 3210–3217. <https://doi.org/10.1557/JMR.1993.3210>.
- Duchosal, A., Werda, S., Serra, R., Leroy, R., Hamdi, H., 2015. Numerical modeling and experimental measurement of MQL impingement over an insert in a milling tool with inner channels. *Int. J. Mach. Tools Manuf.* 94, 37–47. <https://doi.org/10.1016/j.ijmactools.2015.04.003>.
- Franco, P., Estrems, M., Faura, F., 2008. A study of back cutting surface finish from tool errors and machine tool deviations during face milling. *Int. J. Mach. Tools Manuf.* 48, 112–123. <https://doi.org/10.1016/j.ijmactools.2007.07.001>.
- Friedrich, C.R., 2000. Near-cryogenic machining of polymethyl methacrylate for micromilling tool development. *Mater. Manuf. Processes.* 15, 667–678. <https://doi.org/10.1080/10426910008913012>.
- Jun, M.B.G., Joshi, S.S., Devor, R.E., Kapoor, S.G., 2008. An experimental evaluation of an atomization-based cutting fluid application system for micromachining. *J. Manuf. Sci. Eng.* 130. <https://doi.org/10.1115/1.2738961>.
- Krolczyk, G., Maruda, R., Krolczyk, J., Wojciechowski, S., Mia, M., Nieslony, P., Budzik, G., 2019. Ecological trends in machining as a key factor in sustainable production – a review. *J. Cleaner Prod.* 218, 601–615. <https://doi.org/10.1016/j.jclepro.2019.02.017>.
- Li, K.-M., Chou, S.-Y., 2010. Experimental evaluation of minimum quantity lubrication in near micro-milling. *J. Mater. Process. Technol.* 210, 2163–2170. <https://doi.org/10.1016/j.jmatprotec.2010.07.031>.
- Li, G., Yi, S., Li, N., Pan, W., Wen, C., Ding, S., 2019. Quantitative analysis of cooling and lubricating effects of graphene oxide nanofluids in machining titanium alloy Ti6Al4V. *J. Mater. Process. Technol.* 271, 584–598. <https://doi.org/10.1016/j.jmatprotec.2019.04.035>.
- Liao, Y.-S., Li, T.-H., Liu, Y.-C., 2020. An approach to improve cutting performance in micromilling of titanium alloy. *J. Micro Nano-Manuf.* 8. <https://doi.org/10.1115/1.4046560>.
- Loock, F.V., Fleck, N.A., 2018. Deformation and failure maps for PMMA in uniaxial tension. *Polymer* 148, 259–268. <https://doi.org/10.1016/j.polymer.2018.06.027>.
- Maruda, R.W., Krolczyk, G.M., Feldshtein, E., Pusavec, F., Szydłowski, M., Legutko, S., Sobczak-Kupiec, A., 2016. A study on droplets sizes, their distribution and heat exchange for minimum quantity cooling lubrication (MQCL). *Int. J. Mach. Tools Manuf.* 100, 81–92. <https://doi.org/10.1016/j.ijmactools.2015.10.008>.
- Medeossi, F., Sorgato, M., Bruschi, S., Savio, E., 2018. Novel method for burrs quantitative evaluation in micro-milling. *Precis. Eng.* 54, 379–387. <https://doi.org/10.1016/j.precisioneng.2018.07.007>.
- Melkote, S.N., Thangaraj, A.R., 1994. An enhanced end milling surface texture model including the effects of radial rake and primary relief angles. *J. Inst. Eng.* 116, 166. <https://doi.org/10.1115/1.2901927>.
- Mittal, R.K., Kulkarni, S.S., Singh, R.K., 2017. Effect of lubrication on machining response and dynamic instability in high-speed micromilling of Ti-6Al-4V. *J. Manuf. Processes* 28, 413–421. <https://doi.org/10.1016/j.jmapro.2017.04.007>.
- Muñoz-Escalona, P., Maropoulos, P.G., 2015. A geometrical model for surface roughness

- prediction when face milling Al 7075-T7351 with square insert tools. *J. Manuf. Syst.* 36, 216–223. <https://doi.org/10.1016/j.jmsys.2014.06.011>.
- Oliveira, F.B.D., Rodrigues, A.R., Coelho, R.T., Souza, A.F.D., 2015. Size effect and minimum chip thickness in micromilling. *Int. J. Mach. Tools Manuf.* 89, 39–54. <https://doi.org/10.1016/j.ijmactools.2014.11.001>.
- Pourmand, A., Shaegh, S.A.M., Ghavifekr, H.B., Aghdam, E.N., Dokmeci, M.R., Khademhosseini, A., Zhang, Y.S., 2018. Fabrication of whole-thermoplastic normally closed microvalve, micro check valve, and micropump. *Sens. Actuators B Chem.* 262, 625–636. <https://doi.org/10.1016/j.snb.2017.12.132>.
- Rezaei, H., Sadeghi, M.H., Budak, E., 2017. Determination of minimum uncut chip thickness under various machining conditions during micro-milling of Ti-6Al-4V. *Int. J. Adv. Manuf. Technol.* 95, 1617–1634. <https://doi.org/10.1007/s00170-017-1329-3>.
- Sahoo, P., Patra, K., Singh, V.K., Gupta, M.K., Song, Q., Mia, M., Pimenov, D.Y., 2020. Influences of TiAlN coating and limiting angles of flutes on prediction of cutting forces and dynamic stability in micro milling of die steel (P-20). *J. Mater. Process. Technol.* 278, 116500. <https://doi.org/10.1016/j.jmatprotec.2019.116500>.
- Schneider, F., Das, J., Kirsch, B., Linke, B., Aurich, J.C., 2019. Sustainability in ultra precision and micro machining: a review. *Int. J. Precis. Eng. Manuf. Green Technol.* 6, 601–610. <https://doi.org/10.1007/s40684-019-00035-2>.
- Sutter, G., List, G., 2013. Very high speed cutting of Ti-6Al-4V titanium alloy – change in morphology and mechanism of chip formation. *Int. J. Mach. Tools Manuf.* 66, 37–43. <https://doi.org/10.1016/j.ijmactools.2012.11.004>.
- Thepsonthi, T., Hamdi, M., Mitsui, K., 2009. Investigation into minimal-cutting-fluid application in high-speed milling of hardened steel using carbide mills. *Int. J. Mach. Tools Manuf.* 49, 156–162. <https://doi.org/10.1016/j.ijmactools.2008.09.007>.
- Toropov, A., Ko, S.-L., 2003. Prediction of tool-chip contact length using a new slip-line solution for orthogonal cutting. *Int. J. Mach. Tools Manuf.* 43, 1209–1215. [https://doi.org/10.1016/S0890-6955\(03\)00155-X](https://doi.org/10.1016/S0890-6955(03)00155-X).
- Ucun, I., Aslantas, K., Bedir, F., 2013. An experimental investigation of the effect of coating material on tool wear in micro milling of Inconel 718 super alloy. *Wear* 300, 8–19. <https://doi.org/10.1016/j.wear.2013.01.103>.
- Vazquez, E., Gomar, J., Ciurana, J., Rodríguez, C.A., 2015. Analyzing effects of cooling and lubrication conditions in micromilling of Ti6Al4V. *J. Cleaner Prod.* 87, 906–913. <https://doi.org/10.1016/j.jclepro.2014.10.016>.
- Wang, Y.-N., Fu, L.-M., 2018. Micropumps and biomedical applications – a review. *Microelectron. Eng.* 195, 121–138. <https://doi.org/10.1016/j.mee.2018.04.008>.
- Wu, X., Li, L., He, N., 2017. Investigation on the burr formation mechanism in micro cutting. *Precis. Eng.* 47, 191–196. <https://doi.org/10.1016/j.precisioneng.2016.08.004>.
- Yeo, S.H., Ngoi, B.B.K.A., Chua, L.Y., 1997. Ultrasonic deburring. *Int. J. Adv. Manuf. Technol.* 13, 333–341. <https://doi.org/10.1007/BF01178253>.
- Zhang, W., Lin, S., Wang, C., Hu, J., Li, C., Zhuang, Z., Zhou, Y., Mathies, R.A., Yang, C.J., 2009. PMMA/PDMS valves and pumps for disposable microfluidics. *Lab Chip* 9, 3088. <https://doi.org/10.1039/B907254C>.
- Zhou, C., Guo, X., Zhang, K., Cheng, L., Wu, Y., 2019. The coupling effect of micro-groove textures and nanofluids on cutting performance of uncoated cemented carbide tools in milling Ti-6Al-4V. *J. Mater. Process. Technol.* 271, 36–45. <https://doi.org/10.1016/j.jmatprotec.2019.03.021>.